ISTANBUL TECHNICAL UNIVERSITY ★ GRADUATE SCHOOL OF SCIENCE ENGINEERING AND TECHNOLOGY

SUBSONIC WIND TUNNEL DESIGN

M.Sc. THESIS

Zeynep ASLAN

Department of Aeronautics and Astronautics

Aeronautics and Astronautics Engineering Programme

Thesis Advisor: Prof. Dr. Fırat Oğuz EDİS

April 2016

ISTANBUL TECHNICAL UNIVERSITY ★ GRADUATE SCHOOL OF SCIENCE ENGINEERING AND TECHNOLOGY

SUBSONIC WIND TUNNEL DESIGN

M.Sc. THESIS

Zeynep ASLAN
511111172

Department of Aeronautics and Astronautics

Aeronautics and Astronautics Engineering Programme

Thesis Advisor: Prof. Dr. Fırat Oğuz EDİS

April 2016

İSTANBUL TEKNİK ÜNİVERSİTESİ ★ FEN BİLİMLERİ ENSTİTÜSÜ

SESALTI RÜZGAR TÜNELİ TASARIMI

YÜKSEK LİSANS TEZİ

Zeynep ASLAN
511111172

Uçak ve Uzay Mühendisliği Bölümü

Uçak ve Uzay Mühendisliği Programı

Tez Danışmanı: Prof. Dr. Fırat Oğuz EDİS

Nisan 2016

Zeynep Aslan, a **M.Sc.** student of ITU **Graduate School of Science Engineering and Technology** student ID **511111172**, successfully defended the **thesis** entitled **SUBSONIC WIND TUNNEL DESIGN**, which she prepared after fulfilling the requirements specified in the associated legislations, before the jury whose signatures are below.

Thesis Advisor : **Prof. Dr. Fırat Oğuz EDİS** .....
Istanbul Technical University

Jury Members : **Prof. Dr. Mustafa Özdemir** .....
Istanbul Technical University

Yrd.Doç.Dr. Hayri Acar .....
Istanbul Technical University

Date of Submission: 30 March 2016
Date of Defense: 7 April 2016

To my family,

FOREWORD

I sincerely would like to thank my supervisor Prof. Dr. Fırat Oğuz Edis for trusting me with this thesis project. It did not only allow me to regain my experience in the field of Computational Fluid Dynamics, but it was also a great opportunity to gain knowledge about wind tunnels.
I also would like to thank my dear friend Ufuk Özcan for his invaluable support during this thesis project.
I would like to give my thanks to EDS Team as they all had a small part in my achievement.
Finally, I would like to thank Serdar Seçkin for his technical and moral support even though he is thousands of miles away.

March 2016

Zeynep ASLAN
(R&D Engineer)

TABLE OF CONTENTS

Page

ABBREVIATIONS

LDV : Laser Doppler Velocimetry
PIV : Particle Image Velocimetry
VKI : Von Karman Institude
CFD : Computational Fluid Dynamics
CAD : Computer Aided Design
EDS : EDS Hava Uzay Teknolojileri Mühendislik Limited Şirketi
NPL : National Physical Laboratory
TS-1 : Test Section - 1
TS-2 : Test Section - 2
TS-3 : Test Section - 3
k-ε : k-epsilon Turbulence Model
k-ω : k-omega Turbulence Model

SYMBOLS

Re : Reynolds number
M : Mach number
ṁ : Air flow rate
ρ : Air density
A : Area
v : Velocity
D : Diameter
H : Height
W : Width
L : Length
n : Contraction ratio
β : Porosity ratio
ΔP : Pressure loss
K : Pressure loss coefficient
c : Mean velocity
f : Friction factor
C_2 : Pressure-jump coefficient
α : Face permeability
μ : Laminar fluid viscosity
Δm : Thickness of the porous medium

LIST OF TABLES

Page

LIST OF FIGURES

Page

SUBSONIC WIND TUNNEL DESIGN

SUMMARY

In this thesis, wind tunnel design and requirements are investigated in further and CFD simulations are carried out for different designs.

EDS Atmospheric Boundary Layer Wind Tunnel is designed and constructed by EDS Engineers and it is currently being used in order to measure wind forces on buildings. The purpose of this thesis is adapt EDS Wind Tunnel into a wind tunnel with a higher velocity profile in the test section, using the fans and the current contraction design. Three different test section dimensions are considered and investigated with this thesis.

First test section(TS-1) dimensions are decided as 1x2x2 meters. A second contraction is added right after the EDS Wind Tunnel's contraction. Second contraction for TS-1 design is generated using basic splines with a CAD program. First simulations for TS-1 consisted of mesh independency study, turbulence model comparison and contraction shape comparison and desicion. Mesh independency study was carried out with a coarse mesh of 3.9 million cell count and a fine mesh of 5.3 million cell count and the results showed that 3.9 mesh was enough to get stable CFD results. Turbulence model comparison was carried out between the most appropriate two models; k-ε and k-ω models and results showed that two models gave very similar results and it is decided to use k-ε for further simulations because it is more appropriate for swirling flows. Three other contraction shapes (3rd order, 5th order and 7th order polynomial) investigations are added to simple spline design and all four contraction shapes are compared with eachother depending on the CFD simulation results. Selection criteria was the test section inlet flow quality; uniformity and angularity of the flow. Results showed that 7th order polynomial shaped contraction supplied the best flow quality but the flow quality was still not enough for a wind tunnel test section so it is decided to insert a second screen in the settling chamber.

CFD simulations are carried out for the three test section designs TS-1(1x2x2 m), TS-2(0.75x2x2 m) and TS-3(1.5x2x2 m) designs without the diffuser section. Results showed that TS-2 design gave the best test section inlet flow quality results. TS-1 design test section inlet flow quality results were in the allowable range. TS-3 gave the worst results because of the low contraction ratio and were not appropriate for a wind tunnel.

Full CFD simulations are also carried out for the three designs in order to compare pressure losses in the components of the each tunnel. Results showed that TS-3 design had the lowest pressure losses and TS-2 had the highest pressure losses. The narrower the test section dimensions got, the higher the pressure losses became.

Good flow quality results at the test section inlet are achieved for TS-1 and TS-2 designs. It is also decided that blowing type wind tunnels are highly turbulent and settling chamber and contractions might not be enough to reduce turbulence levels.

SESALTI RÜZGAR TÜNELİ TASARIMI

ÖZET

Rüzgar tünelleri günümüzde birçok alanda kullanılmaktadır. Bu tezde rüzgar tünellerinin geçmiş tarihte nasıl olduğuna dair araştırmalar yapılmıştır. Rüzgar tüneli türleri ve komponentleri üzerine literatür araştırmaları yapılmış ve komponentlerin tasarlanırken nelere dikkat edilmesi gerektiği araştırılmıştır.

EDS Mühendisleri tarafından tasarlanan ve inşa edilen EDS Atmosferik Sınır Tabaka Tüneli, bina aerodinamiği araştırmalarında kullanılmaktadır. Bu tez kapsamında, EDS Rüzgar Tüneli kullanılarak, test odasında daha yüksek hızlara çıkabilen rüzgar tünellerinin tasarlanması amaçlanmıştır. Bu rüzgar tünelleri tasarlanırken, EDS Rüzgar Tüneli'nin fanları ve daralma konisinin kullanılmasına karar verilmiştir.

Rüzgar Tüneli konseptinin geçmişi 15. yüzyıla kadar uzanmaktadır. Leonarda Da Vinci'nin görecelik teorisine göre durgun havada hareket eden cisimle, hava akışına karşı duran cisim aynı etkilere maruz kalır. Leonardo Da Vinci aynı zamanda rüzgar hızını ölçen bir anemometre tasarlamıştır. Tasarladığı anemometrede asılı olan bir levha rüzgarın hızı ile hareket edebilmektedir. Levhanın ulaştığı en yüksek noktaya göre rüzgarın hızı/kuvveti ölçülebilmektedir. Rüzgar tünelinin temelleri bu şekilde atılmışken Avrupa ve İngiltere durgun havaya karşı cisimleri hareket ettiren dönen kol düzenekleri tasarlanmış ve araştırmalarda kullanılmıştır. Bu düzeneklerde temel olarak dönebilen bir şaft sistemine bağlı bir kola cisimler takılıp, bu şaft makaralı bir sistemle kendisine bağlı ağırlıklar ile hareket ettirilebilmekte, böylece kola bağlı olan cisim duran havada hareket kaabiliyeti kazanmış olmaktadır. Rüzgar Tünelinin ilk tasarımı ve başarılı testi 19. yüzyılda Francis Wenham tarafından yapılmış olup daha sonra başka bilim adamları tarafından geliştirilmiş ve aerodinamik alanlarınla kullanımı artmıştır. Wright kardeşler 40x40 cm'lik test odasına sahip bir rüzgar tünelini tasarlayıp araştırmalarında kullanmışlardır. Çalışmalarının sonucunda Wright kardeşler tarihteki ilk uçak ile uçuşu gerçekleştirmişlerdir.

Üfleyen(blowing) ve açık çevrim(open-circuit) tipindeki bir rüzgar tüneli girişten çıkışına sırasıyla fan, dinlenme odası, daralma konisi, test odası ve difüzörden oluşur. Fandan çıkan türbülanslı akış dinlenme odası içerisindeki balpeteği ve ızgaralar ile az türbülanslı hale getirilir. Dinlenme odasında genellikle bir adet petekli yapı ve birden fazla ızgara bulunur. Akış daha sonra daralma konisinden geçerek hızlanır ve uniformlaşır. Daralma konilerinin daralma oranları genel olarak 4 ve 10 arasındadır. Daralma konisinden çıkan akış test odasına girer. Test odası girişindeki akışın uniformluğu önemlidir ve sağlanması gereken tasarım kriterleri vardır. Test odası girişindeki havanın hızındaki değişimler, ortalama hıza göre en fazla %0,3, hava akışının açısallığı ise en fazla 0.1° olmalıdır. Test odası içerisine ölçüm yapılacak cisim/prototipler yerleştirilir ve gözlemler ve ölçümler bu bölmede yapılır. Test odasından çıkan akış difüzöre yönlendirilir. Difüzörün tasarım amacı kinetik enerjiyi basınç enerjisine çevirmektir. Test odasından çıkan yüksek hızlı akış yavaşlatılarak bu

bölmeden havaya bırakılır. Difüzör alan oranları genellikle 5:1 ve 6:1 civarında olup kabul edilebilir açılma açısı 5° ve 7° arasındadır.

Yapılan ilk hesaplamalı akışkanlar dinamiği(CFD) çalışmalarında dinlenme odası bir adet petekli yapı ve bir adet ızgara olacak şekilde tasarlanmıştır. Hesaplamalı akışkanlar dinamiği programı içerisinde petekli yapı ve ızgara için kullanılacak girdiler EDS tarafından daha önce yapılan çalışmalardan alınmıştır. Rüzgar Tüneli girişindeki 6 adet fanın hızları, EDS tarafından daha önce yapılan fan akışkanlar dinamiği sonucundan alınmıştır ve eksenel, radyal ve teğetsel hız profilleri olarak programa girilmiştir.

İlk tasarım olarak kullanılan TS-1 tasarımının test odası boyutları 1x2x2 m'den oluşmaktadır. EDS Rüzgar Tüneli'nin daralma konisinden sonra ikinci bir daralma konisi CAD çizim programı kullanılarak simetrik eğrilerle oluşturulmuştur. Bu geometri ile akışkanlar dinamiği için gereken mesh sayısı çalışması, türbülans modeli ve daralma konisi şekli çalışmaları gerçekleştirilmiş olup, karara varılmıştır. Mesh sayısı çalışmaları için 3.9 milyon mesh ile 5.3 milyon mesh karşılaştırılmış ve akışkanlar dinamiği sonuçlarında çok az farklılık olmasından dolayı 3.9 milyon mesh sayısının yeterli olduğu kararına varılmıştır. Aynı şekilde 3.9 milyon meshlik case, iki ayrı türbülans modeli(realizable k-ε ve SST k-ω) kullanılarak simule edilmiştir ve sonuçlar karşılaştırıldığında iki case arasında çok az farklılık olduğu görülmüştür. Türbülans modeli olarak realizable k-ε ile devam edilmeye karar verilmiştir. Basit eğri modeli daralma konisi, literatür araştırmalarında karşılaşılan diğer üç ayrı daralma konisi şekilleri ile birlikte karşılaştırılmıştır. Diğer koni şekilleri 3'üncü, 5'inci ve 7'inci dereceden polinom denkleminden oluşmaktadır. Daralma konileri karşılaştırılırken, seçme kriteri olarak, test odası girişindeki akışın kalitesi(akışın uniformluğu ve açısallığı) göz önünde bulundurulmuştur. Sonuçlar incelendiğinde, 4 ayrı daralma konisi şeklinden en iyi sonuçları 7'inci derecedeki polinom şeklinin verdiği sonucuna varılmıştır. Yine de test odası girişindeki akışın kalitesinin daha da arttırılması gerektiği düşünülmüştür ve bu amaçla dinlenme odasına ikinci bir ızgara konulmasına karar verilmiştir.

TS-1, TS-2 ve TS-3 tasarımlarının difüzörsüz ve dinlenme odasına yerleştirilen ikinci bir ızgara ile hesaplamalı akışkanlar dinamiği simulasyonları yapılmıştır. TS-2 tasarımının test odası boyutları 0,75x2x2 m, TS-3 tasarımın test boyutları da 1,5x2x2 m'dir. Sonuçlar incelenirken test odası girişindeki akışın kalitesi göz önünde bulundurulmuştur. En iyi sonuçlar TS-2 tasarımı için elde edilmiştir. TS-2 tasarımının test odası girişindeki eksenel akış hızının ortalama akış hızına göre maksimum değişimi bazı bölgeler gözardı edildiğinde %0,3'dür. Akışın maksimum geliş açısı ise yine bazı bölgeler gözardı edildiğinde 0.55°'dir. TS-1 için elde edilen sonuçlara test odası girişindeki eksenel akış hızının ortalamaya göre maksimum değişimi %0,8'dir ve akışın maksimum geliş açısı ise 1° olarak elde edilmiştir. TS-3 tasarımı ise en kullanışsız sonuçları vermiştir. Test odası girişindeki eksenel akış hızının ortalama hıza göre maksimum değişimi %2,5 ve akışın açısallığı maksimum 1,2° olarak elde edilmiştir.

TS-1, TS-2 ve TS-3 tasarımlarının difüzör ile birlikte komple rüzgar tüneli akışkanlar dinamiği analizleri yapılmıştır. Tüm "case"ler 4,4 milyon mesh hücresine ulaşmıştır. TS-1 için tasarlanan difüzör 3,38° açılma yarı açısına ve 2,44 difüzör oranına sahiptir. TS-2 için tasarlanan difüzör 4,31° açılma yarı açısına ve 3,25 difüzör oranına sahiptir. TS-3 için tasarlanan difüzör 2,4° açılma yarı açısına sahiptir ve difüzör oranı 1,63'tür. Rüzgar tüneli komponentlerindeki basınç kayıpları göz önünde bulundurulduğunda en

yüksek basınç kaybı dinlenme odasında ve daha sonra difüzörde oluşmaktadır. Difüzörlerde açılma açısı büyüdükçe basınç kayıpları artmaktadır. Aynı şekilde daralma konisinde de daralma açısı arttıkça basınç kayıpları artmaktadır. Gerçekleştirilen analiz sonuçlarına göre tüm rüzgar tüneli için toplam basınç kaybı en dar test odası boyutları sahip olan TS-2 için 581 Pascal, TS-1 için 495 Pascal ve TS-3 için 444 Pascal olarak elde edilmiştir.

Sonuç olarak EDS Rüzgar Tünelinde kullanmak amacı ile üç farklı test odası boyutuna göre gerçekleştirlen tasarımlar akışkanlar dinamiği analizi yardımıyla incelenmiştir. EDS Rüzgar Tüneline ait 6 adet fan, dinlenme odası ve ilk daralma konisi olduğu gibi kullanılacaktır. İkinci daralma konisinin şekli akışkanlar dinamiği analizleri sonucunda test odası girişindeki akışın kalitesine göre karar verilmiştir. Fanlara ait teğetsel hızların yüksek olması akışın dinlenme odasında bir palpeteği ve iki adet ızgara kullanılmasına rağmen akışın düzeltilmesini zorlaştırmıştır. Tüm hesaplamalı akışkanlar dinamiği analizlerinden elde edilen sonuçlara göre daralma oranının yüksek olduğu rüzgar tünellerinde test odası girişindeki akışın kalitesi daha iyi olarak elde edilmiştir ancak bu sefer de toplam basınç kayıpları artmaktadır. Bu yüzden optimum bir daralma oranı seçilerek, gereken sınırlar içerisinde kalınabilir. TS-1 ve TS-2 tasarımları iyi sonuçlar verdiğinden, EDS Rüzgar tünelinin yüksek hızlı rüzgar tüneline dönüştürülmesinde kullanılabilirler. Yeni tasarımlar oluşturulurken, EDS rüzgar tünelinin içerisine büyük köpük malzemelerden kesilen kalıplar yerleştirilebilir. Böylece arzu edildiğinde kolayca EDS Rüzgar Tünelinin eski geometrisine dönülebilinir. Oluşturulan rüzgar tünelindeki keskin köşelerin yuvarlanılması da türbülansın azalmasına yardımcı olacaktır.

Bu tezde rüzgar tünelleri tasarlanmış ve kullanıma uygun olan geometrilen kararlaştırılmıştır. Gelecek çalışmalarda bu tasarımların hayata geçirilmesi ve gerçekleştirilebilecek testlerle de bu çalışmanın validasyonu yapılabilir.

1. INTRODUCTION

Wind tunnels are designed to generate airflows of different airspeeds, relative to a stationary object. With required instrumentation of the object, it is possible to measure aerodynamic forces and pressure distribution to simulate with actual conditions. Wind tunnels are often used in the aerodynamic research area and the main reason for that is because they offer rapid and accurate measurements and are mostly economical.

Wind tunnels are popular to use because the user can easily control the flow conditions within a test section. In the early stages of the design cycle of an aircraft, aerodynamicists use wind tunnels to test the prototypes and gather a large amount of data on the prototype for various forces on the aircraft.

1.1 Purpose of Thesis

The goal of this thesis is to design a wind tunnel of different test section dimensions for multi functional use of EDS Atmospheric Boundary Layer Wind Tunnel. EDS Wind Tunnel will be adapted to the new aerodynamic wind tunnel design when desired. EDS Wind Tunnel is shortly reviewed in Section 1.3.

1.2 Literature Review

Wind tunnels generate airflows with controlled conditions in order to test the models of interest and can be classified depending on either the air supply type or test section velocities. Both classifications are reviewed briefly in following sections.

1.2.1 Historical background

Invention of wind tunnel is considered as a milestone in aerodynamics because it has given the scientists the chance to investigate the fluid flow around different bluff bodies. First idea of testing a physical body against pressurized air flow goes far back in time to Leonardo da Vinci(1452-1519). Leonardo's relativity principle states that moving air against non-moving object is equivalent to moving object in still air(Wind

tunnel principle). He designed an anemometer that measures the wind speed[1]. Da Vinci defined his work as[2]:

"A device for measuring the force of the wind by reading on the quadrant scale the highest point to which the vane, hinged at the top, is blown.

The air moves like a river and carries the clouds with it, just as running water carries all the things that float upon it."

Da Vinci's design is shown in Figure 1.1[2].

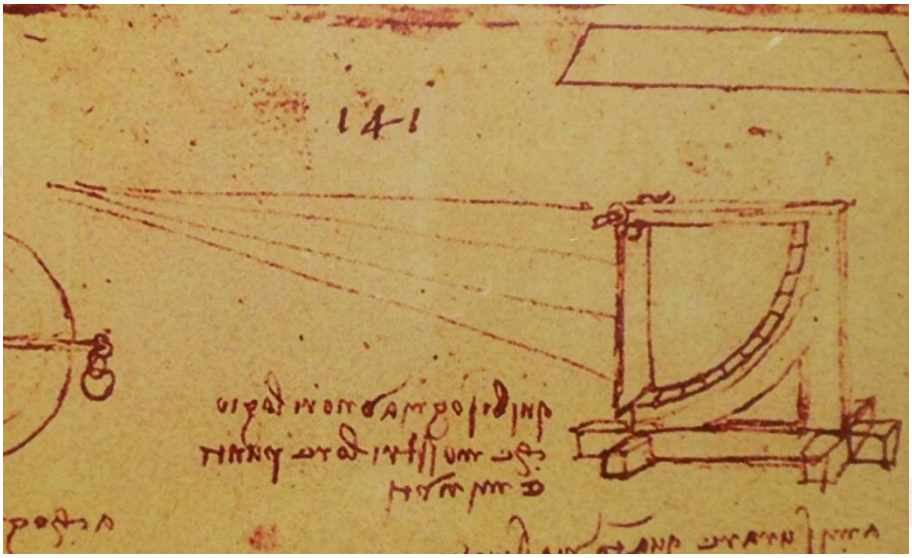

Figure 1.1 : Da Vinci's anemometer design.

An English mathematician Benjamin Robins(1707-1751) designed a machine with the concept of moving objects in still air: whirling arm. This machine had a 1.26 meters long arm that is used to connect to the test object and could spin by a falling weight as illustrated in the Figure 1.2[1]. The velocities that he could reach was only a few feet/secs. This machine made it possible to test different models at some speed in the air. The most important outcome of Robins' work was that air resistance had influential effect on flying objects.

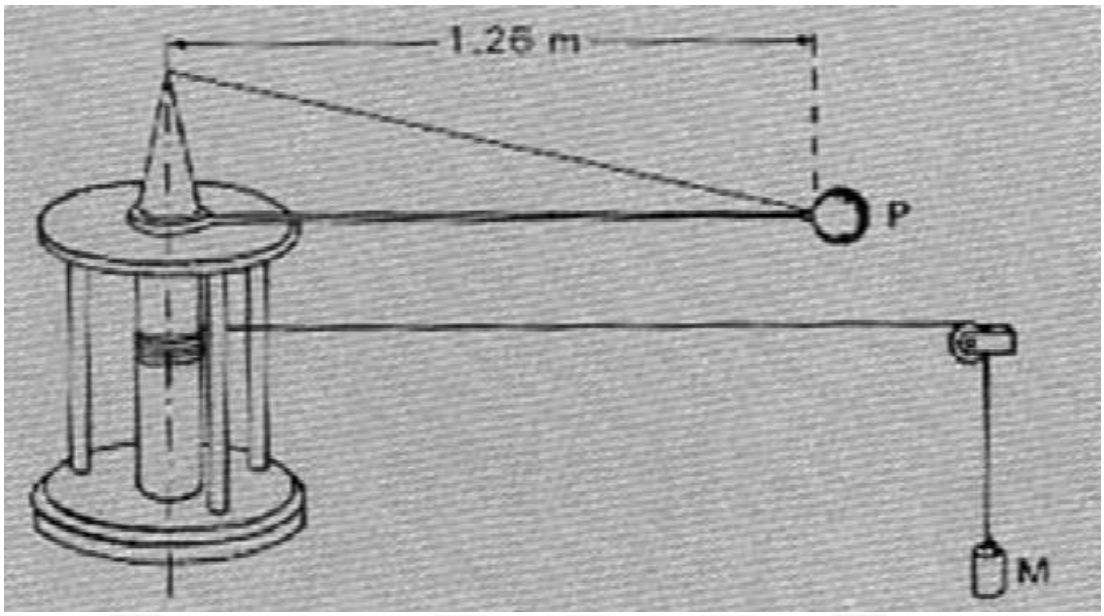

Figure 1.2 : Whirling arm design by Benjamin Robins.

The English scientist Sir George Cayley(1773-1857) invented a whirling arm dedicated only to the study of flight. The arm length that he used was 5 feet and he could reach velocities up to 20 feet/sec. His important conceptual contribution to aerodynamics was separation of propulsion and lift functions. He build a number of unmanned gliders and also created his own concept of an airplane in 1799. Cayley stated that one does not need to have flapping wings as birds in order to be able to fly[1]. His work is displayed as the first research done on airplane aerodynamics.

Modesto Panetti(1875-1957), a professor from Turin Polytecnic created a whirling arm machine that can reach up to transonic velocities[1].

Francis Wenham, a member of the Aeronautical Society of England, contributed the development of the wind tunnel as a marine engineer. He constructed and successfully used the very first wind tunnel in 1871. The wind tunnel had a square test section of 0,46 m and length of 3.6 meter. Wenham discovered inadequacy of Newtonian theory for subsonic flows[1].

Otta Lilienthal(1848-1896) used several whirling arm machines with different arm lengths changing from 2 meters to 7 meters. He succeeded the first manned hang glider flights. He has done about 2500 flights and managed to fly about 250 meters. A picture of Lilienthal from one of this glider flight is shown in Figure 1.3[3].

Figure 1.3 : Otta Lilienthal glider flight.

Sir Hiram Maxim(1840-1916) build larger whirling arm with arm length of 19.5 m and wind tunnel with 0.9 m x 0.9 m x 3.6 m test section dimensions and that can reach up to 22 m/s velocity. He also built a giant flying machine with 3600 kg weight, 370 m^2 wing area, two 180 HP steam engines and 5.4 m diameter propellers[1].

Samuel P. Langley(1834-1906) invented a whirling arm with the arm length of 18.3 that can reach velocities up to 44 m/s. He has also worked on unmanned powered gliders[1].

The Wright Brothers built a complete wind tunnel (Figure 1.4) with a section of area 0.4 m x 0.4 m allowing a maximum wind speed of 60 km/h. With the help of the experiments conducted in the wind tunnel, on December 17^{th} in 1903 Wright brothers managed to fly at Kity Hawk for exactly 59 seconds, covering a distance of 862 feet on the ground[4].

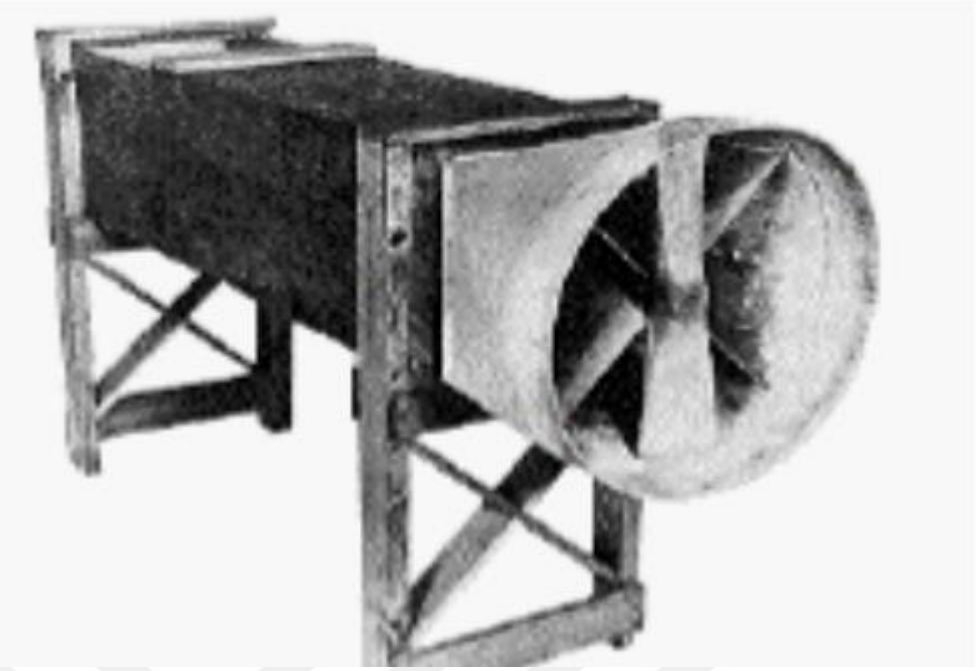

Figure 1.4 : Wright Brothers' wind tunnel.

Wind tunnels for aeronautical applications developed rapidly during the first half of the twentieth century, especially during and between the two world wars. The two basic wind tunnel layouts: the open circuit, or 'N.P.L. (National Physical Laboratory) type', and the closed circuit, or 'Göttingen-type' were developed during this period, named after the research establishments in the U.K. and Germany where they originated. These two types are outlined in the following sections.

In adition to all the flight related work, the first use of a wind tunnel to measure wind forces on buildings is believed to have been made by Kernot in Melbourne, Australia (1893). A sketch of the apparatus, which he called a 'blowing machine', is given in Figure 1.5[5]. This wind tunnel would now be classified as an open-circuit and open test-section type. With this equipment, Kernot studied wind forces on a variety of bluff bodies as cubes, pyramids, cylinders, etc.

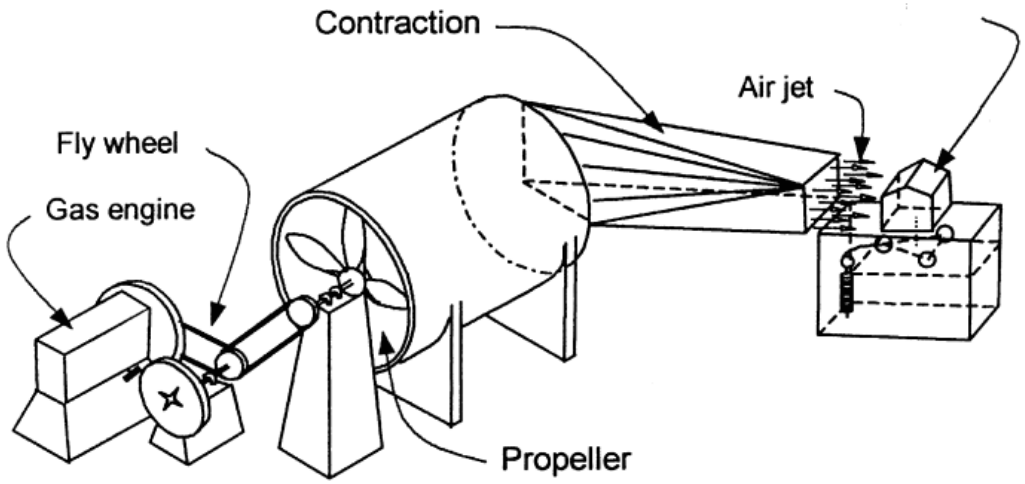

Figure 1.5 : Sketch of Kernot's blowing machine.

1.2.2 Low-speed wind tunnels

Wind tunnels can be classified depending on their test section velocity range. Low-speed tunnels are those with test section velocities less than 180 m/s. Low-speed wind tunnels are further classified into two different types. First type is open circuit tunnels, having no guided return of air, as shown in Figure 1.6[6].

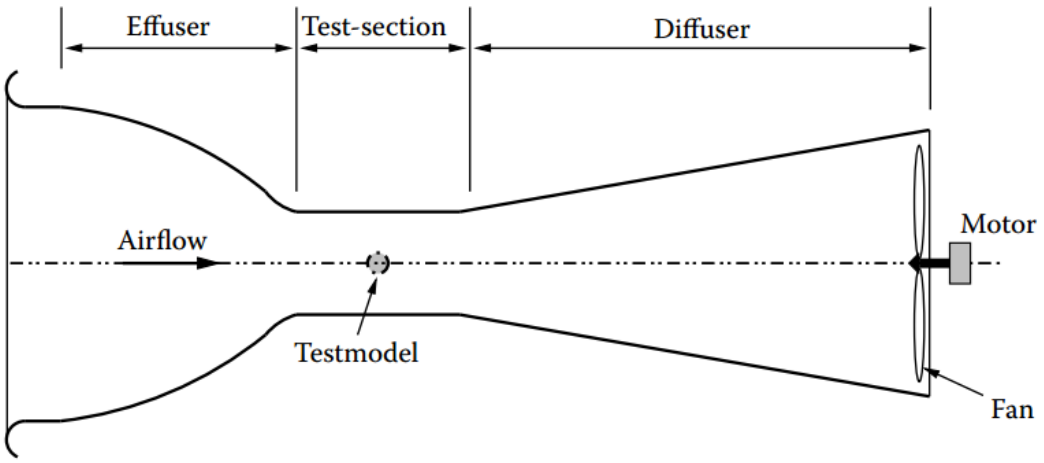

Figure 1.6 : Open-circuit wind tunnel.

After leaving the diffuser, the air circulates by different paths back to the intake. If the tunnel uses air directly from the atmosphere, entirely fresh air flows constantly through the tunnel.

The second type is called closed circuit or return flow tunnel. In this type of tunnel, the air leaving the diffuser uses a continuous path and and returns the test section, as shown in Figure 1.7[6].

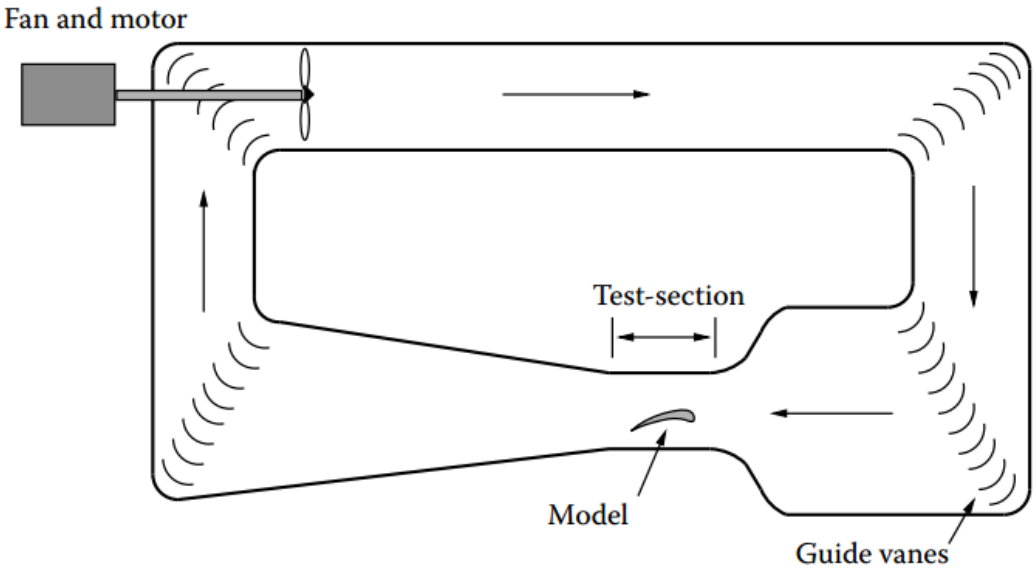

Figure 1.7 : Closed-circuit wind tunnel.

Both open circuit and closed circuit tunnels can operate with either open or closed test-sections. An open test section has no side walls and a closed test section is with side walls. The cross section of the test section can have different shapes such as rectangular, circular, elliptical, octagonal, and so on.

In low speed tunnels, the predominant factors influencing tunnel performance are inertia and viscosity. The effect of compressibility is negligible for these tunnels. Thus, if the Reynolds number of the experimental model and full-scale prototype are equal, any difference in viscosity becomes unimportant.

All modern wind tunnels have four important components: the effuser (the contraction), the working or test section, the diffuser, and the driving unit.

1.2.3 High-speed wind tunnels

Tunnels with test section speed more than 180 m/s are classified as high-speed tunnels. The important point to consider in high speed tunnel operation is that the influence of compressibility is significant. This means that in high speed flows it is essential to consider Mach number as a more appropriate parameter than velocity. A lower limit of high speed might be considered to be the flow with Mach number approximately 0.5 (about 180 m/s) at standard sea level conditions.

Based on the test section Mach number range, the high speed tunnels are also classified as follows.

- 0.8<M<1.2 Transonic tunnel
- 1.2<M<5 Supersonic tunnel
- M>5 Hypersonic tunnel

Similar to low speed tunnels, high speed tunnels are also classified as open circuit tunnels or closed circuit tunnels, based on the type of operation.

1.3 EDS Atmospheric Boundary Layer Wind Tunnel

Wind is air in motion. Obstacles in the path of wind such as buildings and other topographic features deflect or stop wind, converting the wind's kinetic energy into potential energy of pressure, thereby creating wind load.

EDS Wind Tunnel is designed to study how lateral pressures on a building are affected by the velocity of wind, its gradient profile, topographic effects such as hills and escarpments, and the shape and surface features of the building itself. The specifications of the tunnel is listed in Table 1.1 and an image of the tunnel is shown in Figure 1.8[7].

Table 1.1 : EDS wind tunnel specifications.

Tunnel Type	Open Circuit Athmospheric
Test Section Type	Open Section
Test Section Dimensions	2.44 m x 2 m
Max. Velocity	17 m/s
Power Source	6 x 11kW fans

Figure 1.8 : EDS athmospheric boundary layer wind tunnel.

Some velocity measurement tests are performed in the EDS Wind Tunnel's empty test section with the highest fan velocity(1500 rpm) in the vertical direction. These tests helped the staff to understand the velocity field quality and total pressure losses of the wind tunnel. Test section velocity profile in the vertical plane for 1500 rpm fan velocity is shown in Figure 1.9.

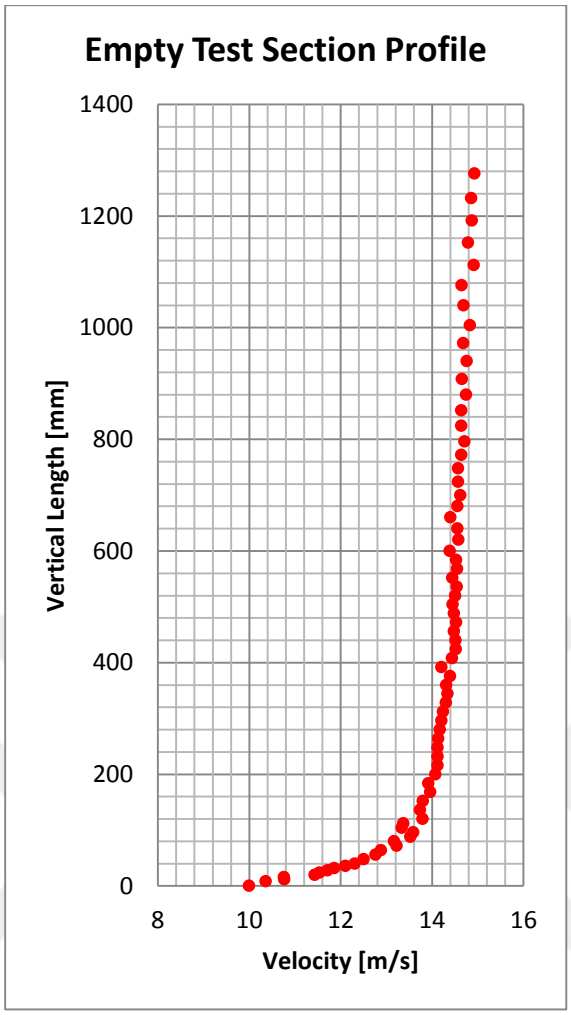

Figure 1.9 : Empty tunnel test section velocity profile @ 1500 rpm fan speed.

EDS Wind Tunnel is an athmospheric boundary layer wind tunnel and that is why the boundary layer thickness is around 200 mm. The entire length of the test section is 15.2 m. Ignoring the boundary layer velocities, values for velocity variation are in the range of 3% from the average.

Approximate mass flow rate of EDS Wind Tunnel is calculated using the velocity profile in Figure 1.9 and the basic equation shown below.

$$\dot{m} = \rho \cdot A \cdot v \tag{1.1}$$

As a result, in order to supply the flow velocity profile shown in Figure 1.9, a fan should generate an air mass flow of approximately 41,500 m^3/h. Following the fan performance curves shown in Appendix A, the tunnel pressure loss should be around 430 Pascal.

2. WIND TUNNEL DESIGN

This thesis aims to design an open circuit subsonic wind tunnel. The wind tunnel will have an upstream fan which means it will be blowing type. This kind of wind tunnel does not have a loop to circulate air and its specific design was developed by Gustav Eiffel in 1909 thus it is also called Eiffel Wind Towel. Advantages and disadvantages of this type wind tunnel is stated below[9].

Advantages of blowing open circuit type wind tunnel:

- Simple design
- Little floor space required
- Accessibility of the wind tunnel
- Any pollutant (smoke flow test, seeding for LDV or PIV measurements or laser sheet visualization, exhaust from engines, water sprays,…) is just blown out
- Always uses fresh air

Disadvantages of this type of wind tunnels are:

- Very bad power factor (loss of kinetic energy at the exit & usually required a wide-angle diffuser)
- Flow leaving the fan may be quite turbulent
- Important noise level
- Always uses fresh air (humid air & no quality control)
- Pressure level in test section can be low because of the leaks

Typical pressure distributions in a blowing open-circuit type wind tunnel is shown in Figure 2.1[8].

In order to achieve the best efficiency and the performance, every component of the wind tunnel has to be designed carefully. In this chapter, important aspects on the wind tunnel design will be reviewed in detail.

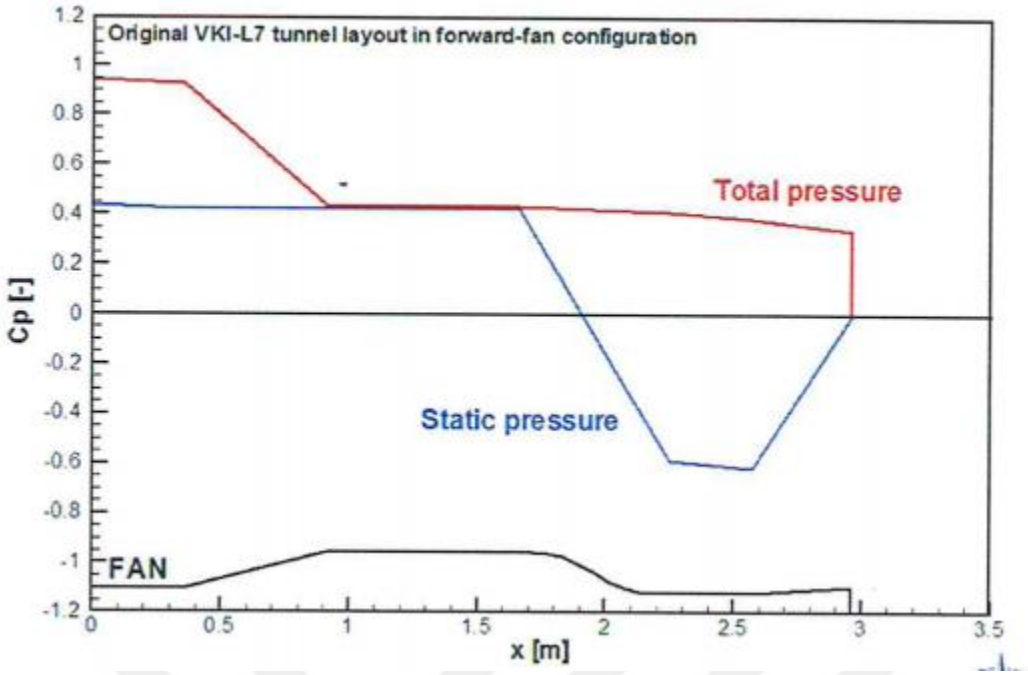

Figure 2.1 : Pressure distributions in an open forward-fan configuration.

2.1 Test-Section

The first step in wind tunnel design is to define the test chamber criterias which are dimensions, shape and desired air velocity. The model that will be tested is placed here in the airflow leaving the downstream end of the contraction, and the required measurements and observations are made here.

If the test section has bounding rigid walls, the tunnel is called a closed throat tunnel. If it is bounded by air at different velocities(usually at rest), the tunnel is called an open jet tunnel. The test section is also referred to as the working section.

According to Barlow and Popes studies, the test chamber length has to be in the range of 0.5-3 times its hydraulic diameter. The air flow exiting the contraction cone needs 0.5 times to hydraulic diameter to become almost uniform. Moreover, a longer test chamber than 3 times the hydraulic diameter could increase boundary layer thickness causing the boundary layer detach at the test chamber exit.

In order to avoid air velocity reduction and an increase in boundary layer thickness at the sharp edges of the test chamber, the sharp edges could be round off.

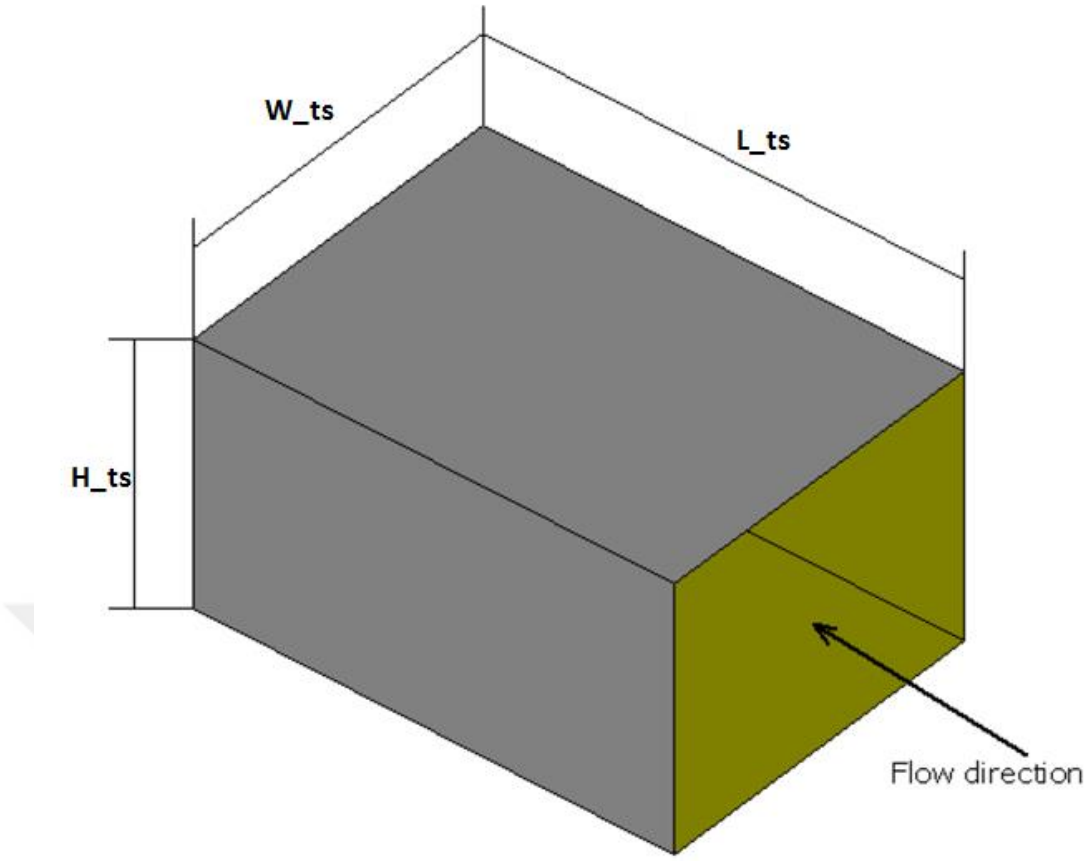

Figure 2.2 : General layout of a three dimensional test section.

Hydraulic diameter for a rectangular shaped duct is defined as:

$$D_h = \frac{4 \cdot H_{ts} \cdot W_{ts}}{2 \cdot (H_{ts} + W_{ts})} \tag{2.1}$$

Values for velocity variation across the test sections of general purpose tunnels are often quoted in the range of 0.20-0.30% variation from the average. Values for angular variation are often quoted in the range of 0.1° from the average flow angle[9].

2.2 The Contraction

The contraction or the "nozzle, as shown in Figure 2.3, is designed to accelerate the flow smoothly to required velocity while providing a uniform flow field in the test section and contributing to turbulence reduction.

In a wind tunnel, the contraction is the most difficult component to design. Flow velocity and its uniformity within the test chamber cross-section depend on the contraction design. The contraction exit cross-section dimensions and shape are

identical to the test chamber ones since they are joined together. The contraction inlet cross-section dimensions and shape are identical to settling chamber exit dimensions.

The contraction ratio is defined as the ratio of the inlet contraction area to outlet contraction area. The contraction ratio should be as large as possible to reduce the total pressure loss through the screens mounted between the settling chamber and the contraction.

$$n = \frac{Area\ at\ entry\ to\ convergent\ cone}{Area\ at\ exit\ of\ convergent\ cone} \tag{2.2}$$

As stated in Pereira J.D.'s work, the contraction ratio usually varies from 4 to 10 for conventional low-speed tunnels[10]. Area ratios greater than 10 lead to excessive inlet dimensions while area ratios less than 6 lead to high pressure loss through the screens.

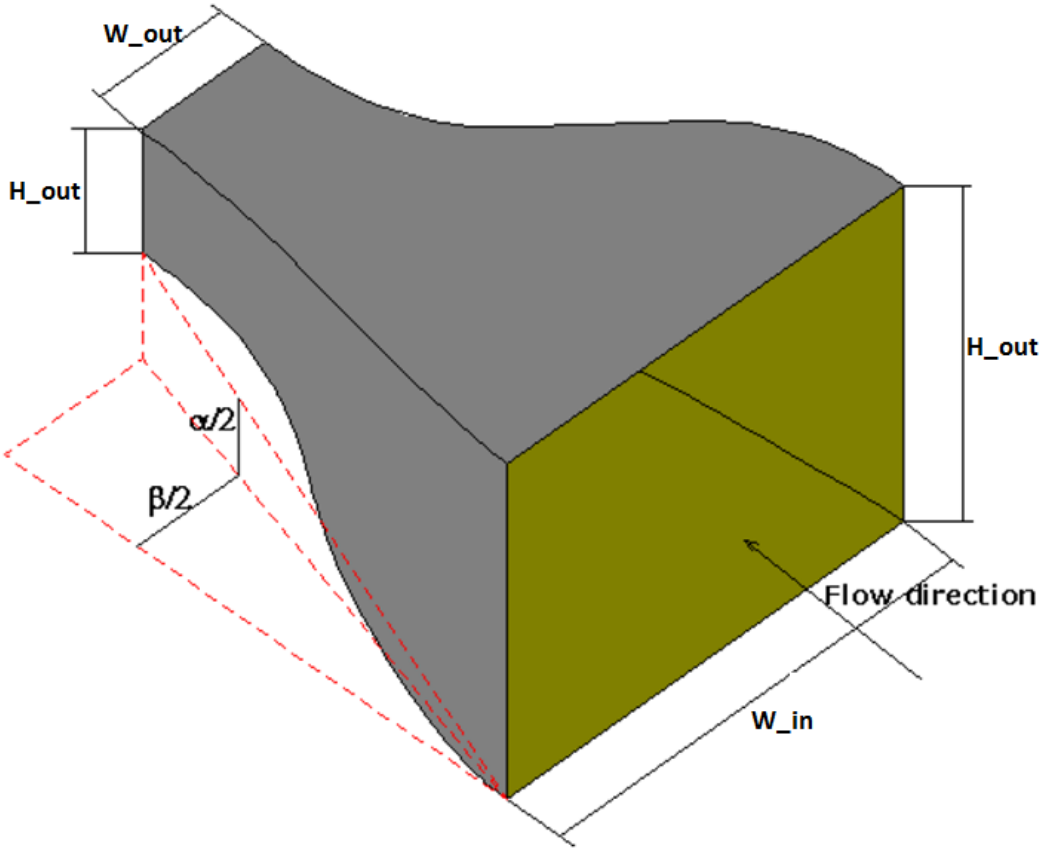

Figure 2.3 : General layout of a three dimensional contraction cone.

Contraction design is important due to transverse pressure gradients and risk of boundary layer seperation. No optimal shape exists for contraction design. Nowadays

CFD (Computational Fluid Dynamics) can be used for this purpose. There are some contraction shapes that can be used such as ;

The VKI classical 7th-order shape

- Simple 7th-order polynomial function
- Extensively used at VKI by Prof. Carnonaro
- Symmetrical curvatures

$$\bar{y} = (-20\bar{x}^3 + 70\bar{x}^2 - 84\bar{x} + 35)\bar{x}^4 \tag{2.3}$$

$$\bar{x} = \frac{L - x}{L} \tag{2.4}$$

$$\bar{y} = \frac{y - y_{out}}{y_{in} - y_{out}} \tag{2.5}$$

The Whitehead, Wu & Waters Shape (1951)

- Hodograph plane approach
- Strong curvature near the contraction exit
- Lehman's fit close to the resulting shape in 2D

$$\frac{D_1}{D_{in}} = 1 - \frac{D_{in} - D_{out}}{D_{in}} \frac{L_1}{L_1 + L_2} \left(\frac{x_1}{L_1}\right)^3 exp\left[\frac{1}{2}\left(1 - \left(\frac{x_1}{L_1}\right)^2\right)\right] \tag{2.6}$$

$$\frac{D_2}{D_{out}} = 1 - \frac{D_{in} - D_{out}}{D_{out}} \frac{L_2}{L_1 + L_2} \left(\frac{x_2}{L_2}\right)^3 exp\left[\frac{1}{2}\left(1 - \left(\frac{x_2}{L_2}\right)^2\right)\right] \tag{2.7}$$

$$\frac{L_1}{L_2} = \frac{D_{in}}{D_{out}} \tag{2.8}$$

The Chmielewski Shape (1974)

- Profile families based on a specified acceleration function
- Inviscid (potential flow) treatment

$$\left(\frac{R_{in}}{R(x)}\right)^4 = (C^2 - 1)\frac{F(x)}{F(L)} + 1 \tag{2.9}$$

$$F(x) = \int_{x_{in}}^{x} \left\{ \frac{1}{2} \left[1 - cos\left(2\pi \left(\frac{\xi}{L} \right)^{n} \right) \right] \right\}^{p} d\xi \qquad (2.10)$$

Comparison of the three different contraction shape is given in Figure 2.4 [8].

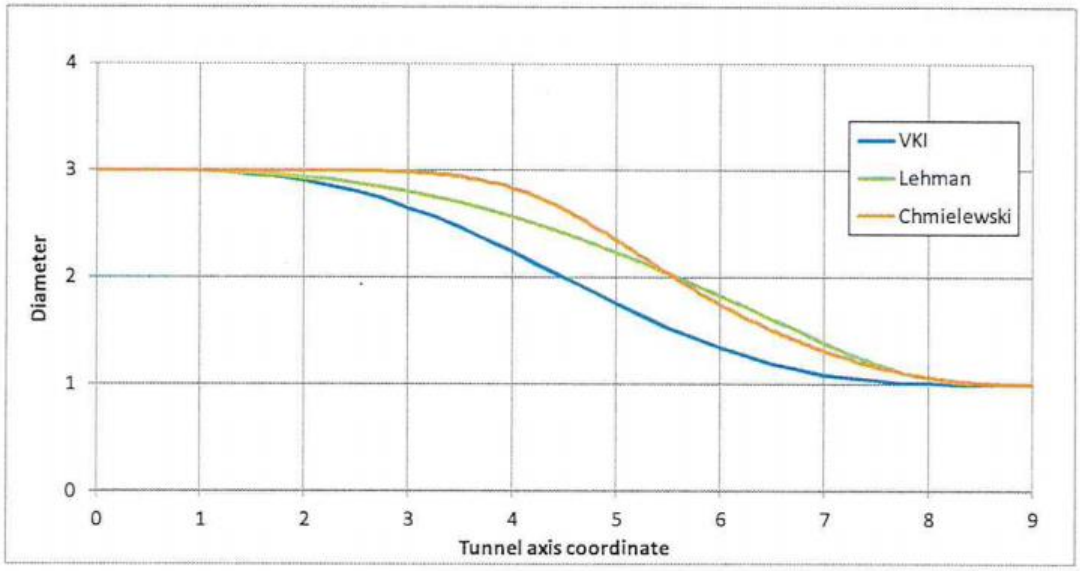

Figure 2.4 : Comparison of three different contraction shape.

A contraction cone should have a total length around contraction inlet width or height.

$$L_{cont} \cong W_{in} \cong H_{out} \qquad (2.11)$$

2.3 Diffuser

The purpose of the diffuser is to convert the kinetic energy of the flow coming out of the test-section to pressure energy, before it leaves the diffuser, as efficiently as possible. Generally, the smaller the diffuser divergence angle, the more efficient is the diffuser.

The inlet cross-section area and shape of the diffuser are known because they equal the cross-section area and shape of the test chamber.

Acceptable diffuser angles are between 5 and 7 degrees. In order to avoid thick boundary layers and promoting seperation, aspect ratios around 5:1 and 6:1 seems to be “the rule”.

2.4 Settling Chamber

A settling chamber is located in front of the contraction cone and usually contains honeycombs and screens to reduce to flow turbulence before it enters the contraction cone.

2.4.1 Honeycomb

A honeycomb with its cells aligned in the flow direction is able to reduce fluctuationg variations in transverse velocity. The honeycomb has little effect on stream-wise velocity due to the fact that the pressure drop through a honeycomb is small.

In the honeycomb design procedure, its length, cell hydraulic diameter, and the porosity are key factors.

Honeycomb porosity (Eq. 2.12) is defined as the ratio of actual flow cross-section area over the total cross-section area.

$$\beta_h = \frac{A_{flow}}{A_{total}} \tag{2.12}$$

Two main criteria have to be verified in wind tunnel honeycomb design. These criterias are expresses by Eq. (2.13) and Eq. (2.14).

$$6 \leq \frac{L_h}{D_h} \leq 8 \tag{2.13}$$

$$\beta_h \geq 0.8 \tag{2.14}$$

2.4.2 Screens

In settling chambers, screens are located after the honeycomb. Screens mainly reduce stream-wise velocity fluctuations, with little effect on flow direction. Instead of only one fine mesh screen, a serious of screens with different mesh qualities are more efficient.

Porosity range for an effective screen should be between 0.58 and 0.8. Screen porosity values over 0.8 are not suitable for good turbulence control, while values below 0.58 lead to flow instability.

Screens could also be installed on a removable frame for cleaning and maintanence.

2.5 Driving Unit

Generally the driving unit consists of a motor and a propeller or fan combination. The fan is used to increase the static pressure of the stream leaving the diffuser.

2.6 Pressure Losses of The Components

In a wind tunnel, pressure losses occur as consecutive pressure losses in the different sections. Overall pressure loss (ΔP_{global}) equals the pressure gain due to the fan.

2.6.1 Pressure losses in a test section

In a wind tunnel component, *i*, pressure loss (ΔP_i) can be written as the product of pressure loss coefficient K_i and the dynamic pressure at the entrance of the component.

$$K_i = \frac{\Delta p_i}{\frac{1}{2} \cdot \rho_i \cdot c_i^2} \tag{2.15}$$

where c_i is the mean velocity (in the section) at the entrance of component *i*.

In order to calculate the test section pressure losses, the test section will be considered as a constant section duct. A flow inside a test section will be turbulent because it is continuous along the whole wind tunnel. The pressure loss coefficient, related to the dynamic pressure in the test section, which is considered as the reference dynamic pressure for all the calculations, is given by the expression below:

$$K_{ts} = \frac{\lambda \cdot L}{D_H} \tag{2.16}$$

where L is the length of the test chamber, D_H the hydraulic diameter and λ is a coefficient given by the expression:

$$\lambda = 1/(1.8 \cdot \log Re - 1.64)^2 \tag{2.17}$$

Where Re is the Reynold number based on the hydraulic diameter.

2.6.2 Pressure losses in a contraction cone

Pressure loss in a contraction cone is considered only due to skin friction. The losses in the contraction is about 3% of total loss and can be expressed as:

$$K_{cont} = 0.32 \cdot f_{av} \cdot \left(\frac{L_{cont}}{D_{sc}}\right) \tag{2.18}$$

where L_n is the contraction length, D_{sc} is the settling chamber hydraulic diameter, and f_{av} is the average friction factor between contraction inlet and outlet sections.

2.6.3 Pressure losses in a diffuser

A simplified procedure for pressure loss calculation in a diffuser is presented here to facilitate a quick estimation of such coefficient.

The pressure loss coefficient, with respect to the dynamic pressure in the narrow side of the diffuser, is given by:

$$K_{diff} = 4 \cdot \tan(\alpha/2) \sqrt[4]{\tan(\alpha/2)} \cdot \left(1 - \frac{A_{in}}{A_{out}}\right)^2 + K_f \tag{2.19}$$

α being the average opening angle, A_{in} the area of the diffuser inlet, A_{out} the area of the diffuser outlet and where K_f is defined as:

$$K_f = \frac{0.02}{8 \cdot \sin(\alpha/2)} \left[1 - \left(\frac{A_{in}}{A_{out}}\right)^2\right] \tag{2.20}$$

2.6.4 Pressure losses in a screens

An empirical relation for the screen loss coefficient is proposed by W.T.Eckert and it is based on three main parameters: porosity, the Reynolds number calculated with wire diameter Re_w and mesh factor K_{mesh}.

$$K_m = K_{mesh} \cdot K_{Rn} \cdot \sigma_s + \frac{\sigma_s^2}{\beta_s^2} \tag{2.21}$$

where;

$$K_{Rn} = \begin{cases} 0.785\left(1 - \frac{Re_w}{354}\right), & 0 \le Re_w < 400 \\ 1.0, & Re_w \ge 400 \end{cases} \tag{2.22}$$

Where Re_Δ is the Reynolds number based on material roughness Δ and D_h is the cell hydraulic diameter.

2.6.5 Pressure losses in honeycombs

To determine the pressure loss in honeycombs, the three main pasameters of stream-wise length to cell hydraulic diameter ratio, porosity and Reynolds number based on cell hydraulica diameter.

$$K_h = \lambda_h \left(\frac{L_h}{D_h} + 3\right)\left(\frac{1}{\beta_h}\right)^2 + \left(\frac{1}{\beta_h} - 1\right)^2 \tag{2.23}$$

where;

$$\lambda_h = \begin{cases} 0.375\left(\frac{\Delta}{D_h}\right)^{0.4} Re_\Delta^{-0.1} , & Re_\Delta \leq 275 \\ 0.214\left(\frac{\Delta}{D_h}\right)^{0.4} , & Re_\Delta > 275 \end{cases} \tag{2.24}$$

3. COMPUTATIONAL FLUID DYNAMICS STUDIES

Three different test section dimensions are considered for this study. The dimensions are listed in Table 3.1.

Table 3.1 : New design test section dimensions.

Test Section Number	Test Section Dimensions (WxHxL)
TS-1	1 x 2 x 2 m
TS-2	0,75 x 2 x 2 m
TS-3	1,5 x 2 x 2 m

3.1 Previous CFD Simulations by EDS Team

While designing and before constractioning of EDS Wind tunnel, EDS Team has completed some CFD simulations in order to decide the final shape of the tunnel and the final fan requirements. Some of these CFD simulations are used and developed in this study.

Fan velocity inlet profiles, that resulted from EDS team's CFD simulations, are used as velocity inlet profiles in each CFD simulation. Axial velocity contours, radial velocity contours and tangential velocity contours of each fan are given in Figure 3.1, Figure 3.2 and Figure 3.3, respectively.

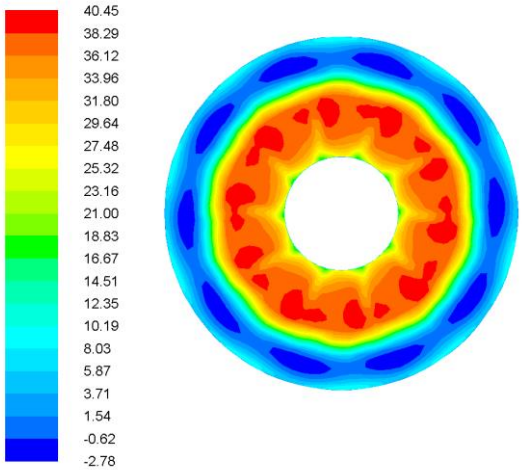

Figure 3.1: Fan axial velocity profile.

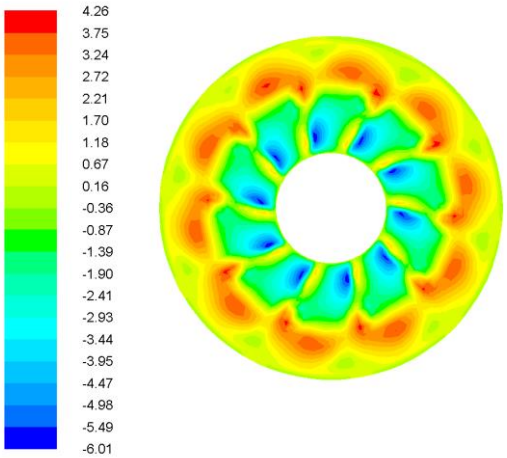

Figure 3.2: Fan radial velocity profile.

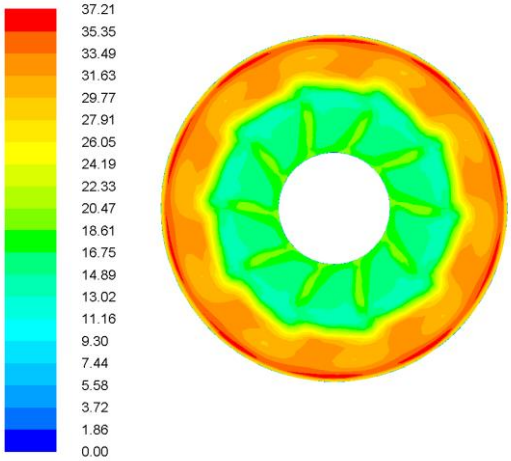

Figure 3.3 : Fan tangential velocity profile.

Honeycomb and screen boundary conditions are copied from the previous CFD simulations as well.

Honeycomb is defined as a porous zone in the CFD solver. The inputs are defined as follows for:

Table 3.2: Porous zone boundary conditions.

Direction-1 Vector	X: 1 Y: 0 Z: 0
Direction-2 Vector	X: 0 Y: 1 Z: 0
Viscous Resistance	D1: Infinite Value D2: Infinite Value D3: C_2
Inertial Resistance	D1: Infinite Value D2: Infinite Value D3: $1/\alpha$
Porosity	A_{holes}/A_{total}

Direction vectors defines the direction that the flow is allowed. Viscous resistance and inertial resistance are supposed to be very high(infinite value) values in the unallowed directions. C_2 (pressure-jump coefficient) can be calculated for honeycomb and screen using pressure loss coefficients(K_L) that are mentioned in Section 2.6.4 and Section 2.6.5 . New pressure loss coefficient is calculated using porosity.

$$K_L' = K_L \frac{v_{x\%open}^2}{v_{100\%open}^2} \tag{3.1}$$

$$C_2 = \frac{K_L'}{thickness} \tag{3.2}$$

Face permeability (α) is calculated using the Darcy's Law as shown in Eq. (3.3)

$$\Delta p = -\left(\frac{\mu}{\alpha} v + C_2 \frac{1}{2} \rho v^2\right) \Delta m \quad (3.3)$$

where μ is laminar fluid viscosity, α is permeability of the medium, C_2 is the pressure-jump coefficient, ν is the velocity normal to the porous face, Δm is the thickness of the medium.

Screen is defined as porous jump in the CFD solver. Boundary conditions are

Table 3.3: Porous jump boundary conditions.

Face permeability	α
Porous medium thickness	Δm
Pressure-jump coefficient	C_2

3.2 CFD Results for TS-1

TS-1 design is considered the main design and more CFD simulations are completed for this design. Mesh independence study, turbulence model comparison and four different contraction shapes are investigated with TS-1 design and the results are presented here.

Tunnel settling chamber, contraction and test section is used in the preliminary simulations. Setling chamber consisted of six fan inlets, one honeycomb and one screen. The contraction shape was a simple spline model and it is investigated further in the following sections with other contraction shapes. Test section dimensions was 1 meter in width, 2 meters in height and 2 meters in length. Considering the velocity profile at the end of the contraction is not uniform enough, test section inlet is accepted 0.5 meter away after the contraction outlet. Therefore the length of the test section can be considered as 1.5 meters.

Some important planes of the wind tunnel is shown in Figure 3.4 and listed in Table 3.4.

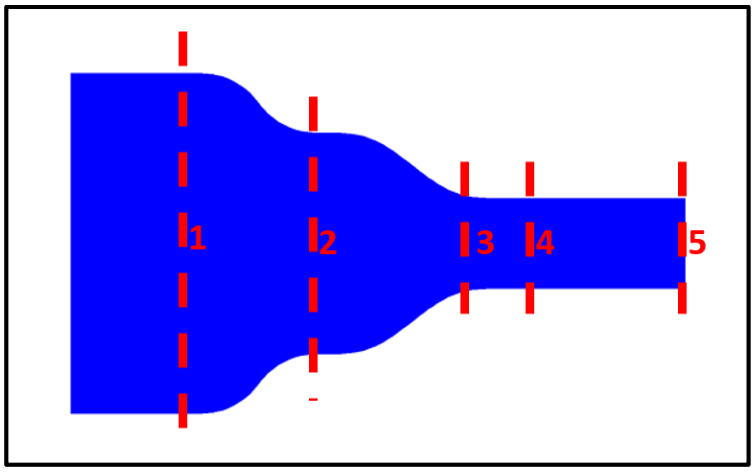

Figure 3.4: Important plane locations.

Table 3.4: Important plane definitions.

Plane Number	Plane Definition
1	First contraction inlet/Settling chamber exit
2	First contraction exit/Second contraction inlet
3	Secons contraction exit
4	Test section inlet
5	Test section outlet

3.2.1 Mesh independence study results for TS-1 design

Turbulence model k-ε is used for this study. Coarse mesh consisted of 3.9 million cells and it is later adapted using the CFD solver and reached up to 5.3 million cells.

Calculated area-weighted average total pressure values on important planes are listed on Table 3.1. From the table, it can be understood that total pressure variations between coarse and fine mesh are below 0.5 Pascal.

Table 3.5 : Area-weighted average calculated total pressure values for mesh independence study.

Plane Definition	**Coarse Case P_{total} [Pa]**	**Fine Case P_{total} [Pa]**
First Contraction Exit Plane	1154.68	1154.50
Second Contraction Exit Plane	1134.32	1134.15
Test Section Inlet Plane	1127.45	1127.38
Test Section Outlet Plane	1112.10	1112.38

Alongside with the total pressure variation, it is importand to investigate variations in velocity field. Velocity magnitude results along the contraction cones and test sections for coarse mesh and fine mesh are showed in Figure 3.5 and Figure 3.6, respectively. The change in variation in velocity magnitude in the global range is neglectable. The area-weighted averaged velocity magnitude on the plane showned in both figures is only 0.01% different for coarse and fine mesh.

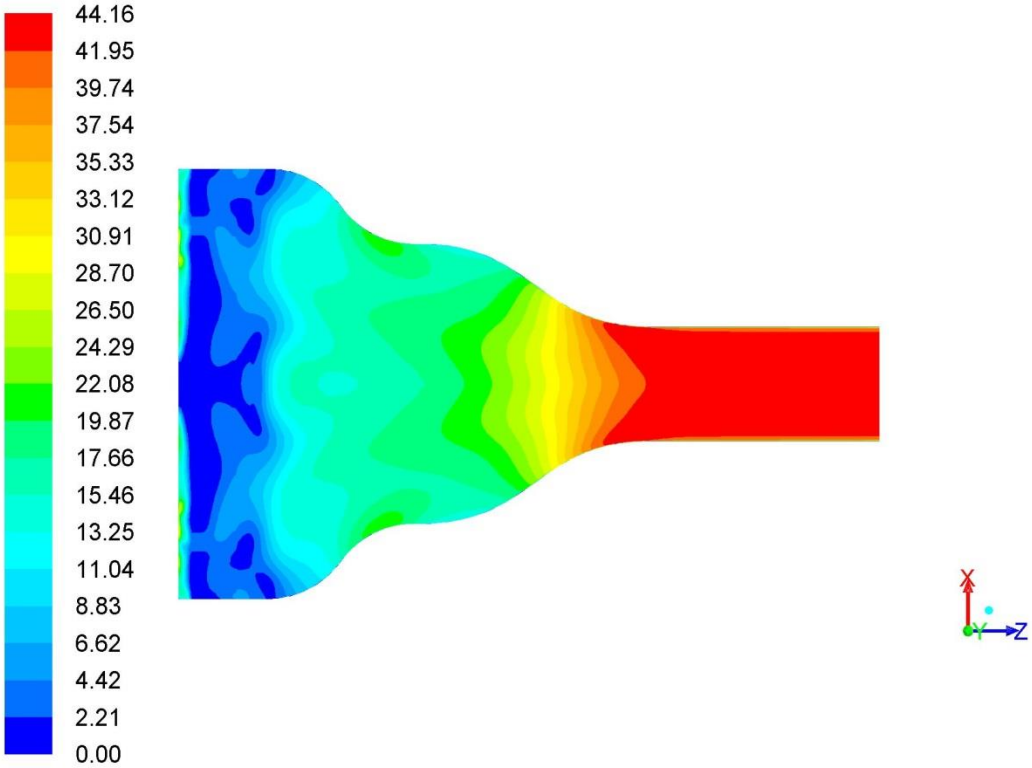

Figure 3.5 : Coarse mesh results – velocity magnitude[m/s].

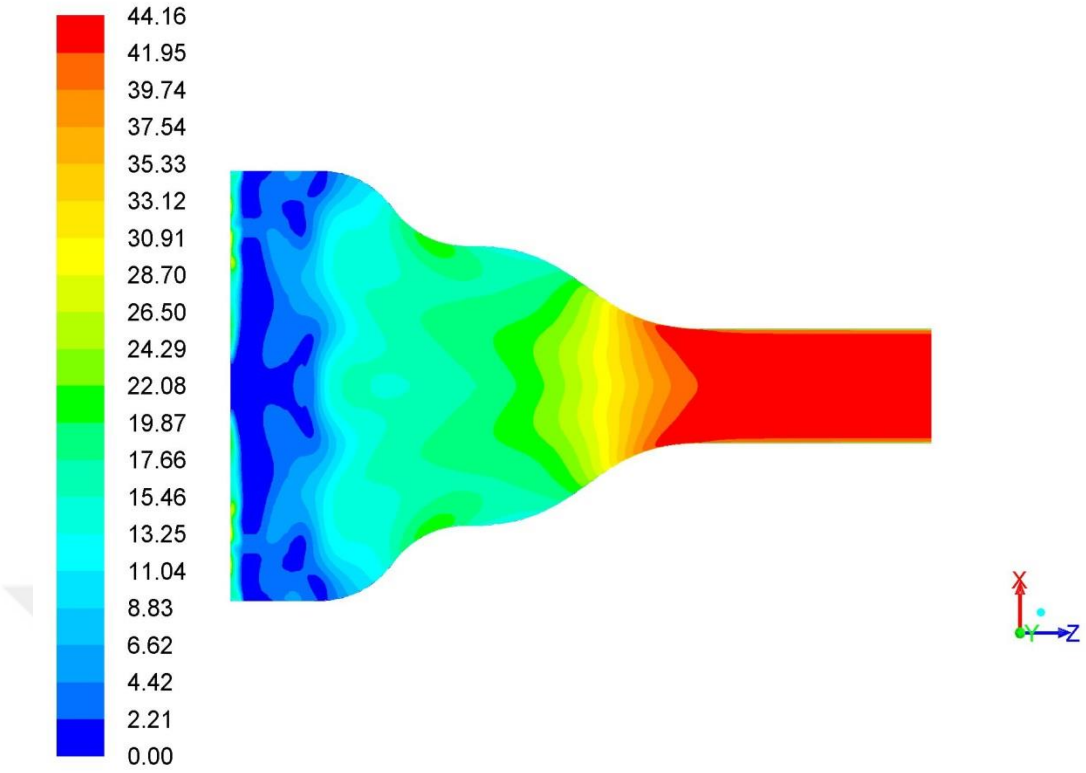

Figure 3.6 : Fine mesh results – velocity magnitude[m/s].

Another important plane to investigate is test section inlet plane. Axial velocity contours are plotted in Figure 3.7 and Figure 3.8 for coarse and fine mesh, respectively. The area-weighted averaged axial velocity variation for two cases is within the range of 0.0001%.

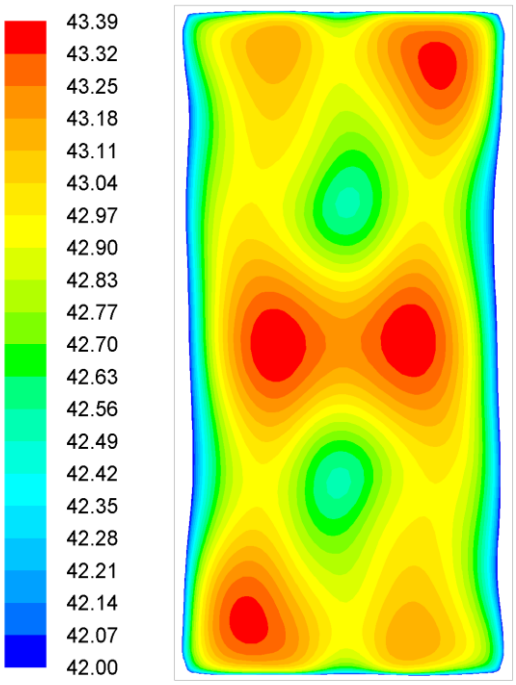

Figure 3.7 : Coarse mesh results.

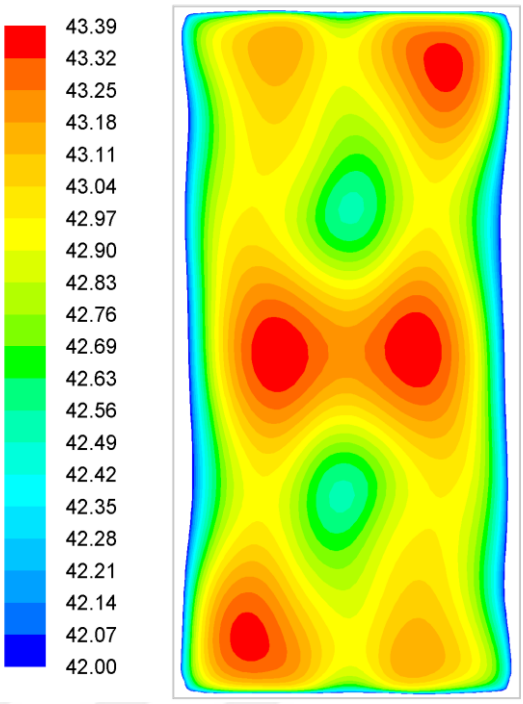

Figure 3.8 : Fine mesh results.

From the results shown, it can be concluded that 3.9 million mesh cells is enough to obtain good CFD results. With this study, it is decided that all the other case meshes will be around 3.9 million cells.

3.2.2 Turbulence model comparison for TS-1 design

Two turbulence models, realizable k-ε and SST k-ω, are compared with TS-1. The results are listed in Table 3.6. From the table, it can be understood that maximum total pressure variation between the two turbulence models is around 3 Pascal.

Table 3.6 : Area-weighted average calculated total pressure values for different turbulence models.

Plane Definition	**k-ε Case P_{total} [Pa]**	**k-ω Case P_{total} [Pa]**
First Contraction Exit Plane	1154.68	1151.45
Second Contraction Exit Plane	1134.32	1134.68
Test Section Inlet Plane	1127.45	1128.15
Test Section Outlet Plane	1112.10	1112.62

Alongside with the total pressure variation, it is importand to investigate variations in velocity field. Velocity magnitude results along the contraction cones and test sections for k-ε turbulence model and k-ω turbulence model are showed in Figure 3.9 and Figure 3.10, respectively. The change in variation in velocity magnitude in the global range is neglectable. The area-weighted averaged velocity magnitude on the plane showed in both figures is only 2% different for k-ε and k-ω turbulence models.

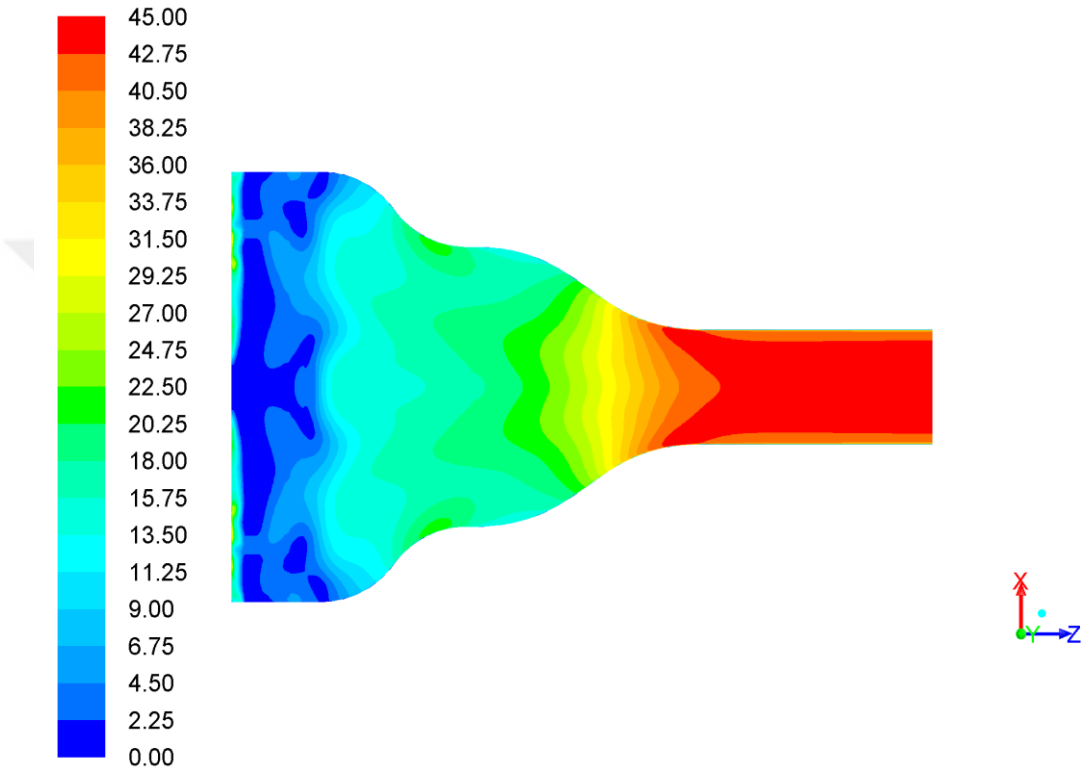

Figure 3.9 : k-ε turbulence model results – velocity magnitude[m/s].

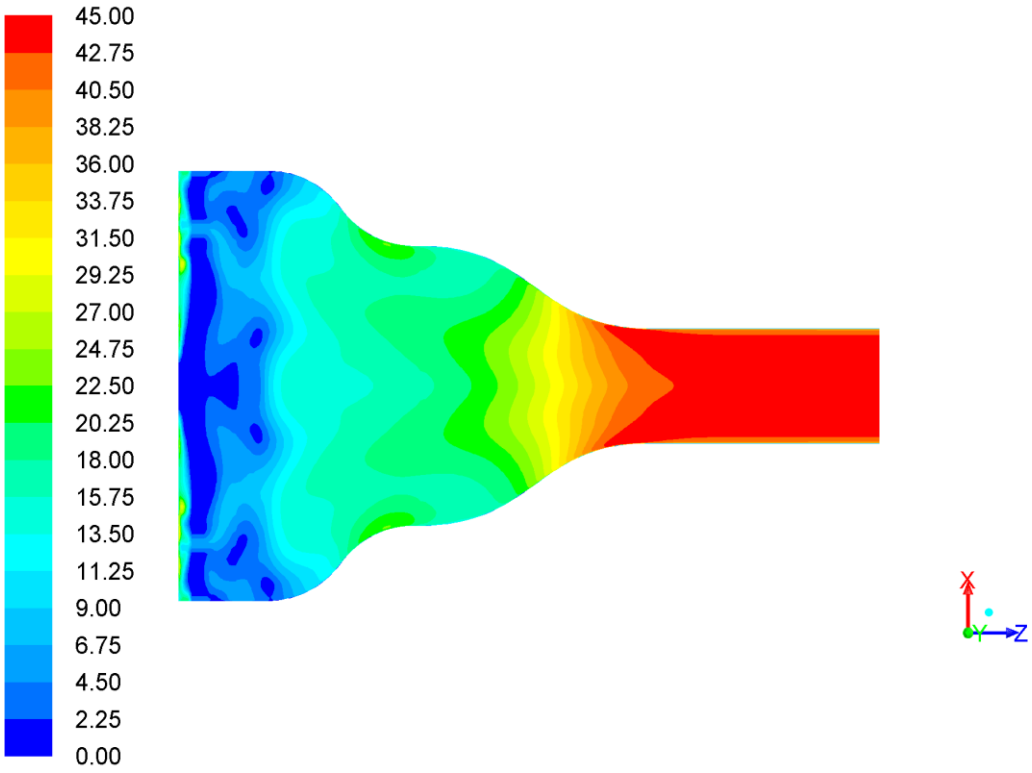

Figure 3.10 : k-ω turbulence model results – velocity magnitude[m/s].

Another important plane to investigate is test section inlet plane. Axial velocity contours are plotted in Figure 3.11 and Figure 3.12 for k-ε and k-ω turbulence models, respectively. The area-weighted averaged axial velocity variation for two cases is within the range of 0.00003%.

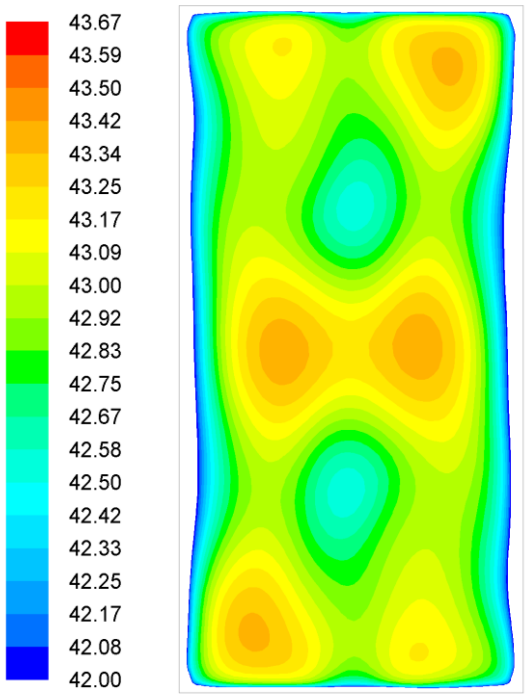

Figure 3.11 : k-ε turbulence model.

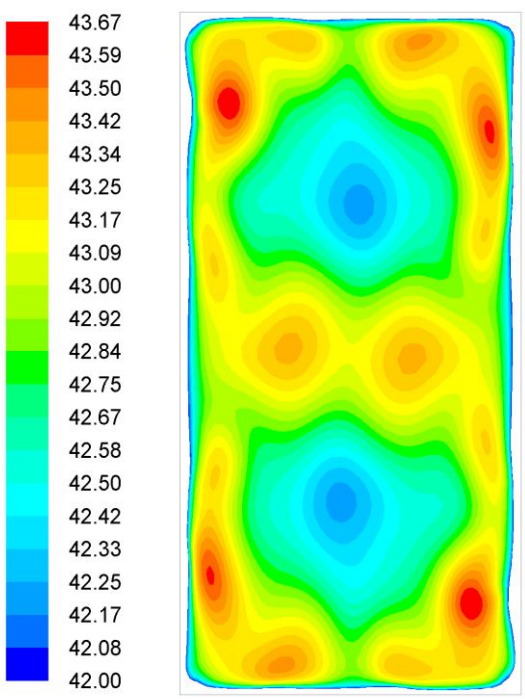

Figure 3.12 : k-ω turbulence model.

The turbulence model for the further CFD simulations is decided as k-ε, because k-ε turbulence model gives better results when dealing with swirling flows. In this study, there are six fan velocity inlets and the flow inside the tunnel is supposed to be swirling because of the fans.

Comparing the results, it is decided that realizable k-ε gave better results but unfortunately, there is no test results to validate CFD results. This might be considered as a further study.

3.2.3 Contraction cone shape results for TS-1

Four different contraction shapes are investigated with TS-1 including the simple spline design. Other three contraction shapes are the third order, fifth order and seventh order polynomial shapes that are defined by Eq. (3.4), Eq. (3.5) and Eq. (3.6), respectively.

$$\bar{y} = (-2\bar{x} + 3)\bar{x}^2 \tag{3.4}$$

$$\bar{y} = (6\bar{x}^2 - 15\bar{x} + 10)\bar{x}^3 \tag{3.5}$$

$$\bar{y} = (-20\bar{x}^3 + 70\bar{x}^2 - 84\bar{x} + 35)\bar{x}^4 \tag{3.6}$$

where;

$$\bar{x} = \frac{L - x}{L} \tag{3.7}$$

$$\bar{y} = \frac{y - y_{out}}{y_{in} - y_{out}} \tag{3.8}$$

Comparison of the four contraction shapes for TS-1 design is showned in Figure 3.13.

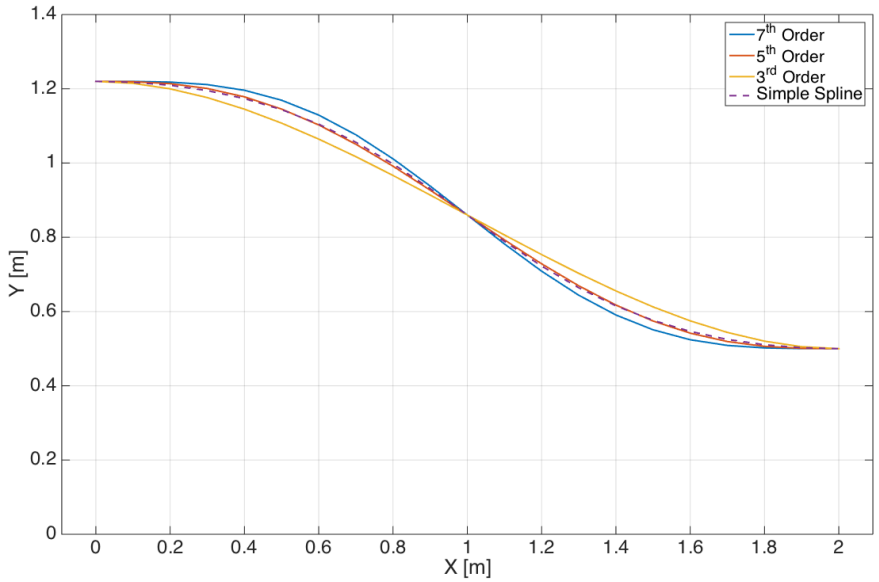

Figure 3.13 : Contraction shape comparison for TS-1 design.

Most important parameters to decide the contraction shape is the uniformity of the flow and relative velocity angle at the test section inlet. As stated before, test section plane starts 0.5 meter after the contraction exit. In order to eliminate boundary layer effects, test section inlet plane is bounded with 10 cm from the sides. Test section inlet flow quality results for the four contraction shapes are listed in Table 3.7.

Table 3.7 : Contraction shape comparison depending on test section inlet velocity quality.

Contraction Shape	Average Velocity [m/s]	Velocity Variation [%]	Rel.Velocity Angle [deg]
Simple Spline Shape	43.012386	+0.008817 Max.	+0.5235262 Max.
		-0.011144 Min.	-0.6105894 Min.
Third Order Polynamial Shape	42.959469	0.008683 Max.	+0.6122148 Max.
		-0.0120661 Min.	-0.6951275 Min.
Fifth Order Polynamial Shape	43.014618	+0.008794 Max.	+0.5101607 Max.
		-0.0107697 Min.	-0.6193516 Min.
Seventh Order Polynamial Shape	43.057941	+0.008761 Max.	+0.4489176 Max.
		-0.0105492 Min.	-0.6164308 Min.

Pressure losses are also another important factor deciding the wind tunnel components. Area-weighted pressure losses are calculated for each contraction design and listed in Table 3.8.

Table 3.8 : Contraction shape comparison depending on the pressure losses.

Contraction Shape	Pressure Loss
Simple Spline Shape	20.367 Pascal
Third Order Polynamial Shape	18.0341 Pascal
Fifth Order Polynamial Shape	21.1153 Pascal
Seventh Order Polynamial Shape	23.3107 Pascal

From Table 3.7, even though there is not a huge difference between the results for all the contraction shapes, it can be decided that 7^{th} order polinomial contraction shape supplies the best flow quality. From Table 3.8, it can be concluded that the 7^{th} order

polynomial contraction shape has the highest pressure loss but it is only 2-3 Pascal difference from the other shapes so it can be neglected.

Axial velocity contours at the test section inlet for 7th order polynomial is showed in Figure 3.14. The axial velocity variations, large boundary layer, velocity relative angles and the axial velocity contour shows that the inlet velocity field should be improved. For this purpose, settling chamber length will be extended and a second screen will be installed at the settling chamber.

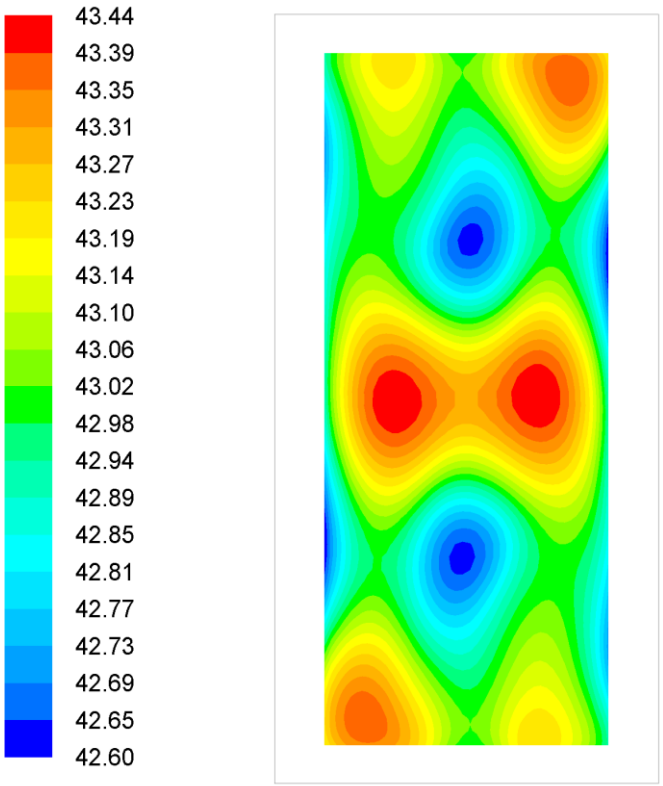

Figure 3.14 : Test section inlet axial velocity contour for 7th order polynomial contraction.

3.3 CFD Results for TS-1

Final CFD results for TS-1 design is presented here. Investigating the previous simulations, it is decided to insert one more screen in settling chamber with the same characteristics. Simulations are carried out with k-e turbulence model.

In order to eliminate the boundary layer effect, test section inlet plane is bounded 5 cm from the sides. The area-weighted averaged axial velocity at the test section inlet is 42.99 m/s. Axial velocity variation contours and relative velocity angle contours at the

test section inlet are given in Figure 3.15 and Figure 3.16, respectively. From Figure 3.15, it can be seen that axial velocity ranges 2.1% maximum. But that is because of the small dark blue areas from the sides. If we ignore those areas, maximum axial velocity variation is around 0.8%. Maximum relative velocity angle is around 1°.

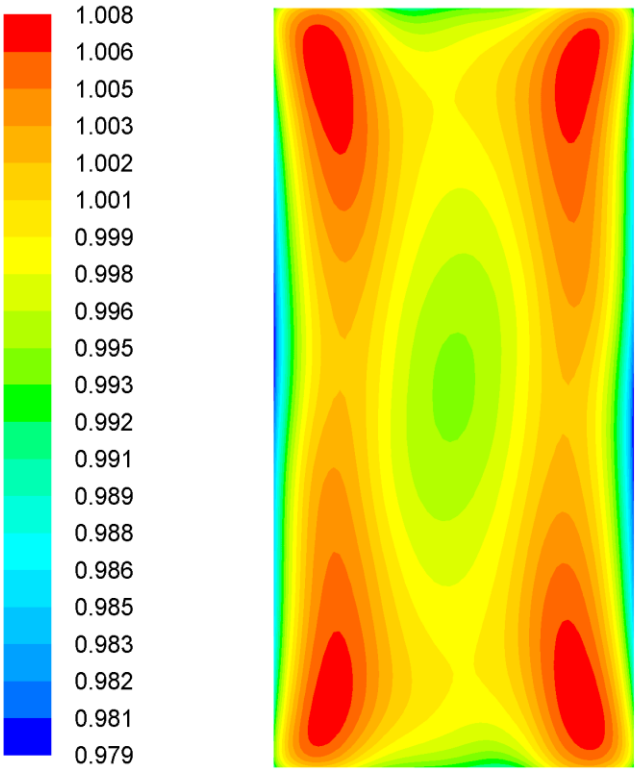

Figure 3.15 : Velocity variation at the test section inlet of TS-1.

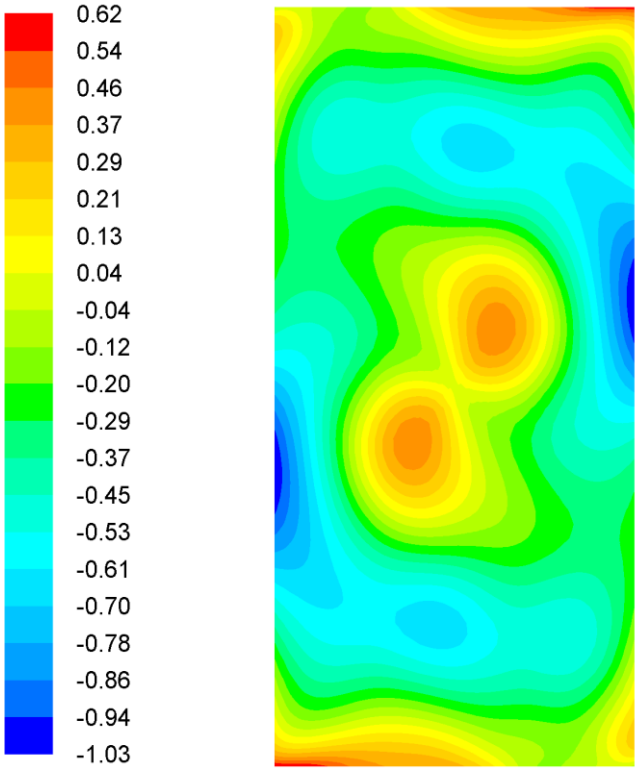

Figure 3.16 : Relative velocity angle at the test section inlet of TS-1.

3.4 CFD Results for TS-2

TS-2 design consists of a 6 fan velocity inlets, one honeycomb and two screens, a 7th order polynamial contraction shape and a test section of 0.75 x 2 x 2 m. Boundary conditions are the same with the TS-1 design simulations.

Similar to TS-1, in order to eliminate the boundary layer effect, test section inlet plane is bounded 5 cm from the sides. The area-weighted averaged axial velocity at the test section inlet is 57.42 m/s. Axial velocity variation contours and relative velocity angle contours at the test section inlet are given in Figure 3.17 and Figure 3.18, respectively. From Figure 3.17, it can be seen that axial velocity ranges 1% maximum. But that is because of the small dark blue areas from the sides. If we ignore those areas, maximum axial velocity variation is around 0.3%. Maximum relative velocity angle is around 0.55°.

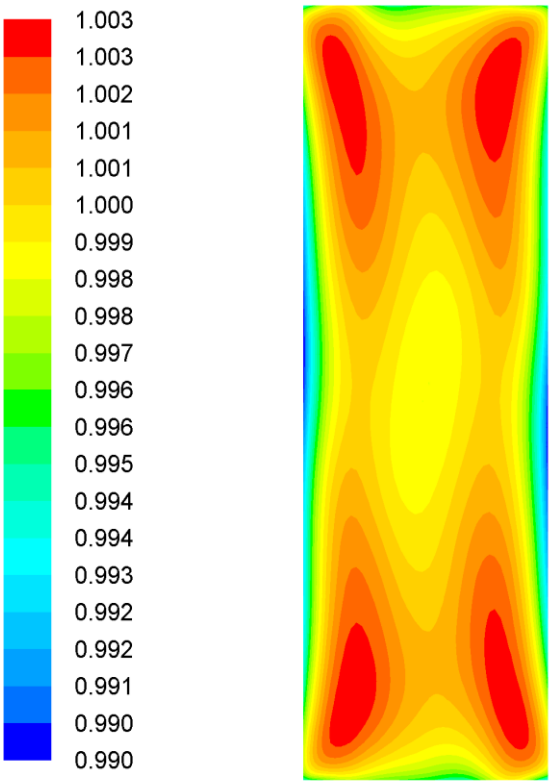

Figure 3.17 : Velocity variation at the test section inlet of TS-2.

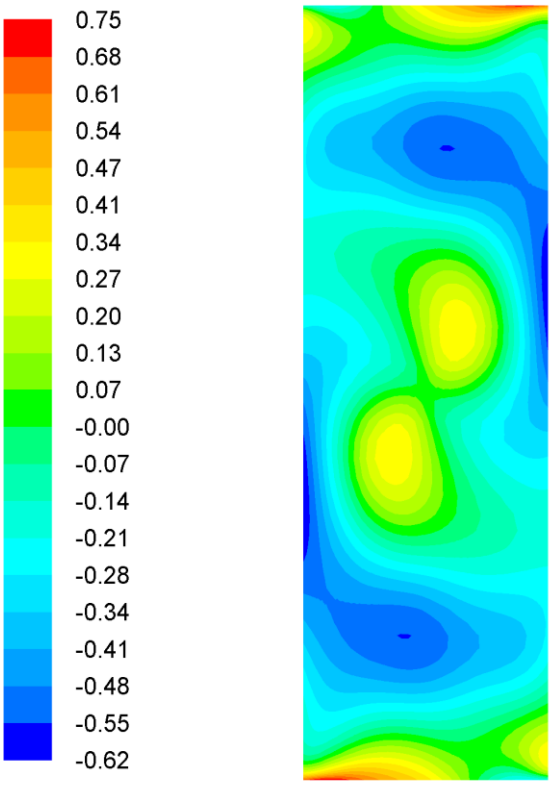

Figure 3.18 : Relative velocity angle at the test section inlet of TS-2.

3.5 CFD Results for TS-3

TS-2 design consists of a 6 fan velocity inlets, one honeycomb and two screens, a 7th order polynamial contraction shape and a test section of 1.5 x 2 x 2 m. Boundary conditions are the same with the TS-1 design simulations.

Similar to TS-1 and TS-2, in order to eliminate the boundary layer effect, test section inlet plane is bounded 5 cm from the sides. The area-weighted averaged axial velocity at the test section inlet is 28.6 m/s. Axial velocity variation contours and relative velocity angle contours at the test section inlet are given in Figure 3.15, respectively. From Figure 3.19, it can be seen that axial velocity ranges 5% maximum. The reason for the high variation is the small dark blue areas from the sides. If we ignore those areas, maximum axial velocity variation is around 2.1% which is still pretty high. Maximum relative velocity angle is around 1.2°.

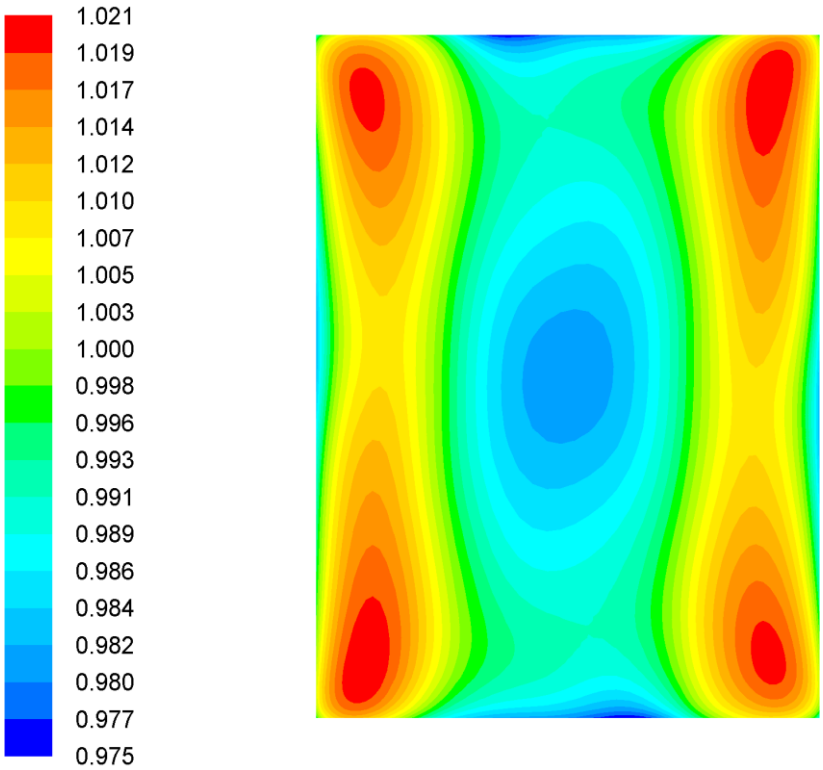

Figure 3.19 : Velocity variation at the test section inlet of TS-3.

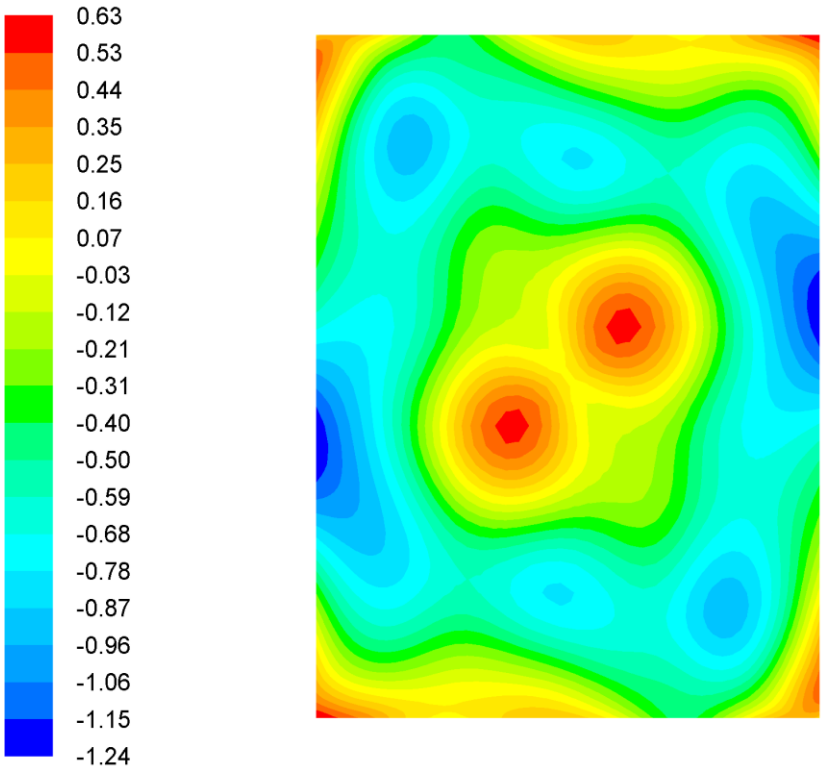

Figure 3.20 : Relative velocity angle at the test section inlet of TS-3.

Comparing all the results from TS-1, TS-2 and TS-3, it is obvious that the TS-2 design gave the best results and it still needs to be improved. TS-1, TS-2 and TS-3 designs have contraction ratio of 2.44, 3.25 and 1.63, respectively. In Section 2.2, it is stated that contraction ratio should be between 4 and 10. Contraction ratios of all the designs are smaller than 4, so this might be the reason why the axial velocity variation contours and relative velocity angle contours did not improve better even after inserting the second screen. Another reason might for this might be that the test section does not have a square or circular shape. It is harder to design rectangular test sections.

3.6 Full Wind Tunnel CFD Results

After finalizing the screen number and contraction shape, full CFD simulations are carried out for all three designs, including a diffuser starting at the outlet of the test section. Even though diffusers had the same length for all three designs, they had different inlet/outlet area ratio and angles.

3.6.1 Full wind tunnel CFD results for TS-1

Final CFD simulations consisted of the full tunnel geometry including a diffuser with an outlet/inlet area of 2.44 and an half angle of 3.68° on the horizontal direction only. Axial velocity contours inside the full tunnel for TS-1 design is shown in Figure 3.21. Area-weighted averaged total pressure losses of the tunnel components are listed in Table 3.9.

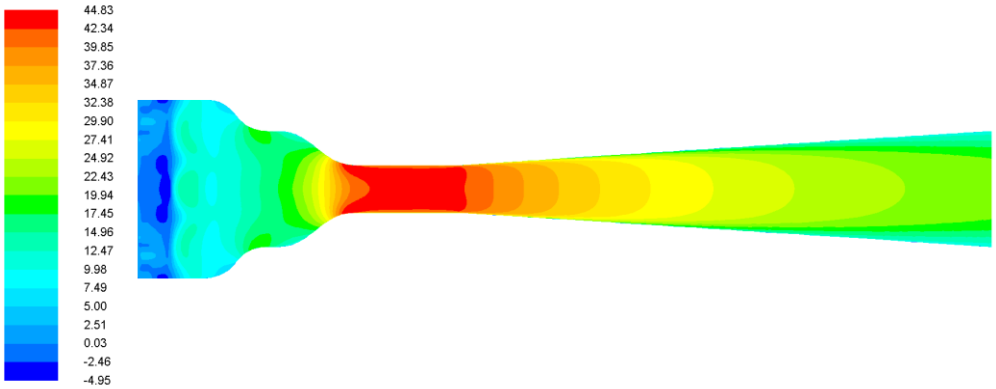

Figure 3.21 : Full tunnel axial velocity [m/s] contours for TS-1 design.

3.6.2 Full wind tunnel CFD results for TS-2

Final CFD simulations consisted of the full tunnel geometry including a diffuser with an outlet/inlet area of 3.25and an half angle of 4.31° on the horizontal direction only. Axial velocity contours inside the full tunnel for TS-2 design is shown in Figure 3.22Figure 3.21. Area-weighted averaged total pressure losses of the tunnel components are listed in Table 3.9.

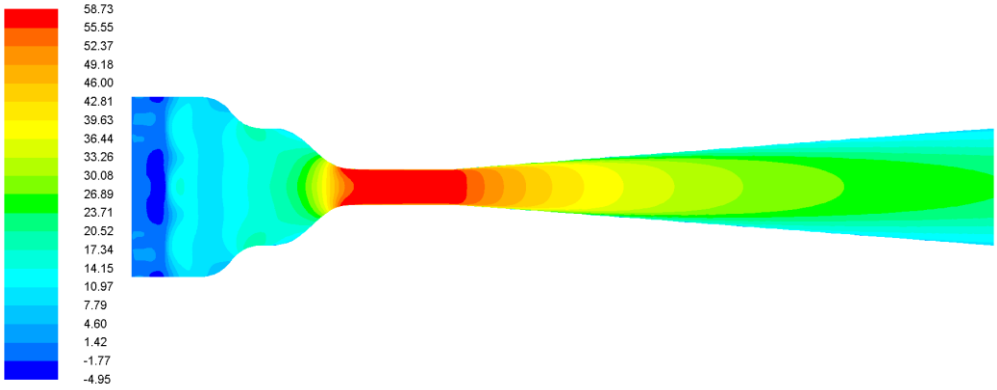

Figure 3.22 : Full tunnel axial velocity [m/s] contours for TS-2 design.

3.6.3 Full wind tunnel CFD results for TS-3

Final CFD simulations consisted of the full tunnel geometry including a diffuser with an outlet/inlet area of 1.63 and an half angle of 2.4° on the horizontal direction only. Axial velocity contours inside the full tunnel for TS-3 design is shown in Figure 3.23Figure 3.21. Area-weighted averaged total pressure losses of the tunnel components are listed in Table 3.9.

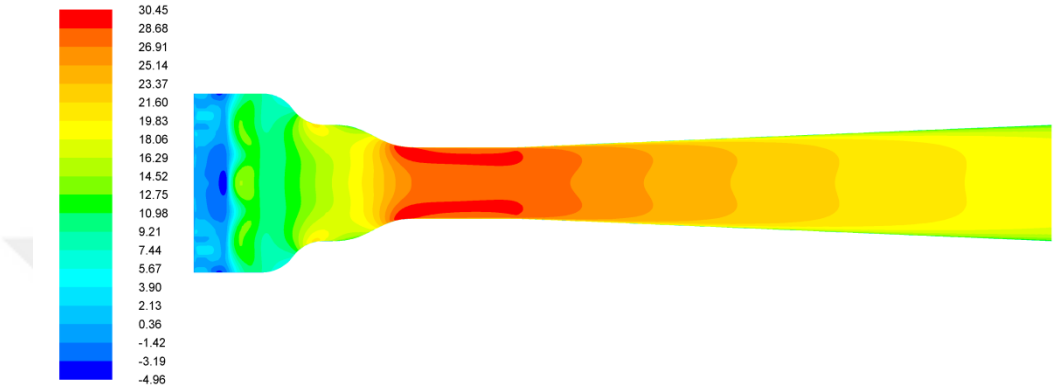

Figure 3.23 : Full tunnel axial velocity [m/s] contours for TS-3 design.

Area-weighted pressure losses are calculated for each component of the TS-1, TS-2 and TS-3 and listed on the Table 3.9.

Table 3.9 : Pressure losses in wind tunnel components.

	TS-1	**TS-2**	**TS-3**
Settling Chamber	398 Pa	397 Pa	398 Pa
Contraction 1	8 Pa	9 Pa	9 Pa
Contraction 2	27 Pa	50 Pa	10 Pa
Test Section	16 Pa	32 Pa	6 Pa
Diffuser	46 Pa	93 Pa	21 Pa
TOTAL	495 Pa	581 Pa	444 Pa

Full CFD simulations are also carried out for the three designs in order to compare pressure losses in the components of the each tunnel. Results showed that TS-3 design

had the lowest pressure losses and TS-2 had the highest pressure losses. The narrower the test section dimensions got, the higher the pressure losses became.

4. DISCUSSION

Three different wind tunnel designs with different test section dimensions are investigated in order to adapt into EDS Atmospheric Boundary Layer Wind Tunnel. Six fans, settling chamber and the first contraction of the tunnel is the ones that were used for EDS Wind Tunnel. In the current design, after the fans, settling chamber and the contraction, a second contraction, a test section and a diffuser is inserted in the model. The three test section dimensions consists of 0.75x2x2 m(TS-2), 1x2x2 m(TS-1) and 1.5x2x2 m(TS-3). Second contraction shape of the tunnel is decided as a result of the test section inlet flow quality comparison between third, fifth and seventh order polynomial shapes. CFD simulations with and without diffuser are carried out for the three different wind tunnel designs.

Fan velocities are inserted in the CFD solver as axial, radial and tangential velocity profiles. Velocity profiles are the results of a previous fan CFD simulation by EDS Team. It should be emphasized that the tangential velocities of the fan are almost as high as the axial velocities which in conclusion generate more turbulent flow in the settling chamber. Since the wind tunnel type is blowing type and the air exiting from the fans is sent to the test section inlet, it is extremely important to reduce the turbulence levels to an appropriate level. In the final CFD simulations, even though a honeycomb and two screens are used in the settling chamber, flow quality at the test section inlet were still higher than the desired values.

Results showed that the contraction ratios are lower than the general design values. Acceptable results are achieved for TS-1 and TS-2 designs. Best results are gained for TS-2 design which has the highest contraction ratio of 3.25. Finally sharp edges inside the wind tunnel could be round off to help to reduce the turbulence levels.

EDS Wind Tunnel can be turned into the new design when desired.

REFERENCES

[1] Carbonaro, M. (2015). Overview of Wind Tunnels, *Lecture Series, Introduction to Ground Testing Facilities,* von Karman Institude for Fluid Dynamics, Belgium, 3–5 November.

[2] Url-1 < *http://themarineinstallersrant.blogspot.com.tr/2014/04/da-vinci-da-boat-da-interpretation.html* >, date retrieved 22.11.2015

[3] Url-1 <*http://www.lilienthal-museum.de* >, date retrieved 22.11.2015.

[4] Dalal, V. (n.d.). Designing and Construction of Low-Speed Wind Tunnel WiWu, Lulea University of Technology.

[5] Holmes, J. D. (2001). Wind Loadings of Structures, Spon Press

[6] Rathakrishnan, E. (2007). Instrumentation, Measurements, and Experiments in Fluids, CRC Press

[7] Url-2 <*http://www.edshavauzay.com/tr/wp-content/uploads/2014/05/tunel.png*> , date retrieved 23.11.2015

[8] Botin, B. (2015). Conventional Wind Tunnels, *Lecture Series, Introduction to Ground Testing Facilities,* von Karman Institude for Fluid Dynamics, Belgium, 3–5 November.

[9] Barlow J. B., Rae W.H.Jr.-Pope A. (1999). Low Speed Wind Tunnel Testing, Wiley Press

[10] Pereira, J.D. (2011). Wind Tunnels: Aerodynamics, Models and Experiments, Noya Science Publishers, Inc

APPENDICES

APPENDIX A: Fan Performance Curves

APPENDIX A

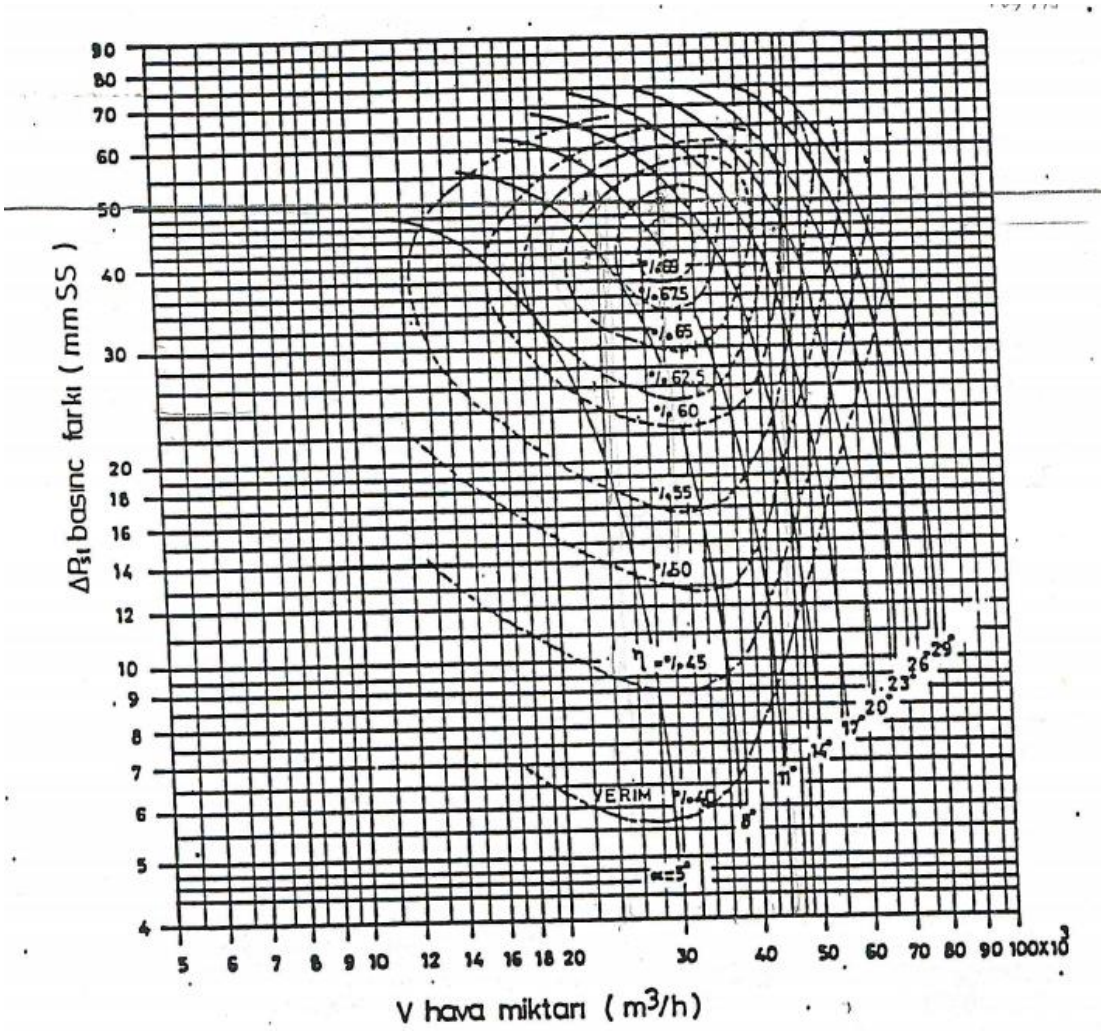

Figure A. 1: Fan performance curves.

CURRICULUM VITAE

Name Surname: Zeynep Aslan

Place and Date of Birth: Alaçam, 25.05.1990

E-Mail: aslanz@itu.edu.tr

EDUCATION:

B.Sc.: Astronautical Engineering